BUREAU OF RECLAMATION

An Eco-Hydraulic Numerical Model for Flows with Complex In-Stream Structures

Science and Technology Program
Research and Development Office

Final Report No. ST-2021-1734-01
Technical Report No. ENV-2021-120

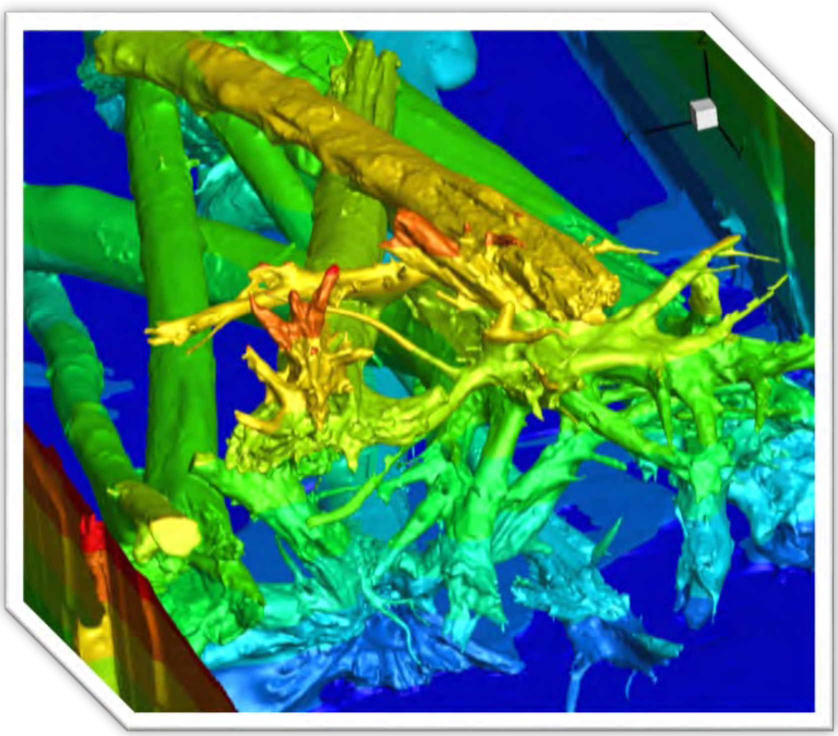

U.S. Department of the Interior

September 2021

Mission Statements

The U.S. Department of the Interior protects and manages the Nation's natural resources and cultural heritage; provides scientific and other information about those resources; and honors its trust responsibilities or special commitments to American Indians, Alaska Natives, and affiliated Island Communities.

The mission of the Bureau of Reclamation is to manage, develop, and protect water and related resources in an environmentally and economically sound manner in the interest of the American public.

Disclaimer

Information in this report may not be used for advertising or promotional purposes. The data and findings should not be construed as an endorsement of any product or firm by the Bureau of Reclamation, Department of Interior, or Federal Government. The products evaluated in the report were evaluated for purposes specific to the Bureau of Reclamation mission. Reclamation gives no warranties or guarantees, expressed or implied, for the products evaluated in this report, including merchantability or fitness for a particular purpose.

Acknowledgements

The Science and Technology Program, Bureau of Reclamation, sponsored this research. This project was carried out in collaboration with internal and external engineers and scientists. Significant contribution and participation in the model development by Prof. Xiaofeng Liu and his students, the Penn State University, are acknowledged.

An Eco-Hydraulic Numerical Model for Flows with Complex In-Stream Structures

Final Report No. ST-2021-1734-01
Technical Report No. ENV-2021-120

prepared by

Yong G. Lai, Ph.D., Hydraulic Engineer
Sedimentation and River Hydraulics Group
Technical Service Center

REPORT DOCUMENTATION PAGE			*Form Approved* *OMB No. 0704-0188*

The public reporting burden for this collection of information is estimated to average 1 hour per response, including the time for reviewing instructions, searching existing data sources, gathering and maintaining the data needed, and completing and reviewing the collection of information. Send comments regarding this burden estimate or any other aspect of this collection of information, including suggestions for reducing the burden, to Department of Defense, Washington Headquarters Services, Directorate for Information Operations and Reports (0704-0188), 1215 Jefferson Davis Highway, Suite 1204, Arlington, VA 22202-4302. Respondents should be aware that notwithstanding any other provision of law, no person shall be subject to any penalty for failing to comply with a collection of information if it does not display a currently valid OMB control number.
PLEASE DO NOT RETURN YOUR FORM TO THE ABOVE ADDRESS.

1. REPORT DATE *(DD-MM-YYYY)*	2. REPORT TYPE	3. DATES COVERED *(From - To)*
30-09-2021	Research	10/2017-09/2021

4. TITLE AND SUBTITLE	5a. CONTRACT NUMBER
An Eco-Hydraulic Numerical Model for Flows with Complex In-Stream Structures	XXXR4524KS-RR4888FARD1802901/FA875
	5b. GRANT NUMBER
	5c. PROGRAM ELEMENT NUMBER 1541 (S&T)
6. AUTHOR(S) Yong G. Lai, Ph.D., Hydraulic Engineer 303-445-2560	5d. PROJECT NUMBER Final Report ST-2021-1734-01
	5e. TASK NUMBER
	5f. WORK UNIT NUMBER

7. PERFORMING ORGANIZATION NAME(S) AND ADDRESS(ES)	8. PERFORMING ORGANIZATION REPORT NUMBER
Sedimentation and River Hydraulics Group Technical Service Center, Bureau of Reclamation Denver, CO 80225	ENV-2021-120
9. SPONSORING/MONITORING AGENCY NAME(S) AND ADDRESS(ES)	**10. SPONSOR/MONITOR'S ACRONYM(S)**
Science and Technology Program Research and Development Office Bureau of Reclamation U.S. Department of the Interior Denver Federal Center PO Box 25007, Denver, CO 80225-0007	Reclamation 11. SPONSOR/MONITOR'S REPORT NUMBER(S) ST-2021-1734-01

12. DISTRIBUTION/AVAILABILITY STATEMENT
Final Report may be downloaded from https://www.usbr.gov/research/projects/index.html

13. SUPPLEMENTARY NOTES

14. ABSTRACT
A new surface embedding method (SEM) is developed and implemented into a 3D computational fluid dynamics (CFD) model U^{2}RANS. The modeling procedure is proposed so that 3D CFD modeling of flows through complex instream structures may be carried out for eco-hydraulic projects. All components of a CFD package to perform the CFD modeling are described. The new capability is described and verified using selected benchmark cases. In specific, a turbulent flow around a cylinder near scoured bed is used to validate the model. Good results are obtained. Further, a complex flow through a six-piece ELJ is used to demonstrate that the model works well even for complex flows. The ELJ case is further lab-tested by collaborators at the U.S. Army Corp of Engineers. The experimental data are further used to validate the model with good comparisons. Addition details of the research have been documented comprehensively in a theory paper (Appendix A) and comparison paper (Appendix B).

15. SUBJECT TERMS
3D CFD Model; Immersed Boundary Method; Instream Structures; Large Wood

16. SECURITY CLASSIFICATION OF:			17. LIMITATION OF ABSTRACT	18. NUMBER OF PAGES	19a. NAME OF RESPONSIBLE PERSON
				68	Yong Lai
a. REPORT	b. ABSTRACT	THIS PAGE			19b. TELEPHONE NUMBER *(Include area code)*
U	U	U			303-445-2560

Standard Form 298 (Rev. 8/98)
Prescribed by ANSI Std. Z39.18

Peer Review

Bureau of Reclamation
Research and Development Office
Science and Technology Program

Final Report No. ST-2021-1734-01

Report Title: An Eco-Hydraulic Numerical Model for Flows with Complex In-Stream Structures

YONG LAI Digitally signed by YONG LAI Date: 2021.09.21 17:23:00 -06'00'

Prepared by: Yong G. Lai
Ph.D. and Hydraulic Engineer
Sedimentation and River Hydraulics Group, 86-68240
Technical Service Center

BENJAMIN ABBAN Digitally signed by BENJAMIN ABBAN Date: 2021.09.21 20:15:21 -06'00'

Peer Review by: Ben Abban
Ph.D. and Hydraulic Engineer
Sedimentation and River Hydraulics Group, 86-68240
Technical Service Center

Contents

Executive Summary

Three-dimensional (3D) computational fluid dynamic (CFD) simulation is gaining popularity in recent years for stream flow modelling. It is necessary when local flow patterns are of interest or there exist instream structures. Representation of complex terrain, however, is a major obstacle in 3D CFD modelling. Traditionally, the surface-conforming method (SCM) is widely used in which the surface is accurately represented by a 3D mesh; i.e., the mesh conforms to the surface geometry. A drawback of the SCM is that such a mesh is difficult to generate when the surface is complex. The mesh quality may become too poor to maintain solution stability and accuracy. An alternative is the surface-embedding method (SEM) in which surface is embedded in a background mesh. The background mesh may be generated without the requirement of conforming to the surface so that mesh generation is relatively simple with good mesh quality. A special algorithm, however, is needed to take into account the effect of the embedded surface on the nearby flow.

In this research, a new method is proposed and developed with the SEM method which is implemented in a 3D CFD model U^2RANS. The research is an effort to address various priority issues facing the large wood (LW) installation at Reclamation river restoration sites. The priority issues of LW structures were discussed and determined at a Reclamation and U.S. Army Corp of Engineers (USACE) Workshop in 2012. A collaborative effort with the objective of determining the feasibility of using suitable computational modeling tools for LW installation has since started.

Key accomplishments of the project are summarized below:

- A comprehensive literature review has been conducted.

- A special SEM has been developed and implemented into U^2RANS in collaboration with multiple partners, in particular, Prof. Xiaofeng Liu at the Penn State University, and David Smith at the U.S. Army Corp of Engineers (USACE).

- A CFD modeling procedure was proposed so that 3D CFD modeling of flows through complex instream structures using SEM may be carried out for eco-hydraulic projects.

- The enhanced 3D model is described and verified using selected benchmark cases. The model is further modified and validated at Reclamation. In specific, a turbulent flow around a cylinder near scoured bed is used to test and validate the model. Further, a complex flow through a 6-piece ELJ is used to demonstrate that the model works for complex flows. The ELJ case is further constructed and lab-tested by the collaborator at USACE. The experimental data are used to validate the model further.

The research results have been documented in scientific journal papers (see Appendices). Future research needs are also discussed.

1. Introduction

Instream structures such as fish structures and large woods are widely used by Reclamation in river management for improving stream flow conditions to enhance fish passage and increase fish habitat areas. Existing design methods or guidelines are based on empirical observations and qualitative analysis; not based on predictive numerical models for a quantitative analysis for their effectiveness at a specific site. Physical responses of streams to the placement of instream structures are rarely analyzed, leading to a lack of evaluation of risk and liability of these in-stream features prior to the project implementation. Many projects, however, need to have data related to the effectiveness, risk and liability for planning, design and implementation. For such quantitative analysis, numerical modeling has been identified as one of the best alternatives.

A wide range of numerical models have been developed and applied in hydraulic engineering for stream restoration applications. They, however, are primarily based on the one-dimensional (1D) and depth-averaged two-dimensional (2D) models. For a recent review on 1D, 2D and hydrostatic-based three-dimensional (3D) models, readers are referred to Lai and Wu (2019).

3D computational fluid dynamic (CFD) flow models, without the hydrostatic pressure assumption, have not been widely used in ecohydraulic analysis for streams with complex instream structures; such models, however, are required since vertical velocity is not negligible and dynamic pressure is nonzero and varies significantly. In this report, such models are named 3D CFD models, to be distinguished from the hydrostatic-assumption 3D models. There are several technical difficulties associated with these CFD models. A key issue is the need to generate a high-quality 3D mesh which is indeed a very difficult task, if not impossible, for fluid flows around structures such as large woods.

In recent years, semi-automatic 3D mesh generation tools have been developed and used for 3D mesh generation. For example, the mesh generation tool snappyhexmesh, called SHM in this report, offered through the open-source model OpenFOAM has been widely used. SHM has been adapted and adopted for modeling applications at Reclamation in recent years (e.g., Lai and Bandrowski 2014). Despite some success, it was found that the existing semi-automatic tools such as SHM were not robust enough – that is, the success of mesh generation was problem-dependent in that it worked for some flow scenarios while failed in other cases pending on the complexity of the instream structure geometry. It is the unpredictability of the 3D mesh generation success that has motivated the present research and development: new and novel methods are needed to overcome the mesh generation robustness issue. Without a good-quality 3D mesh, 3D CFD modeling will not be successful for routine engineering applications.

In this research, a novel immersed boundary (IB) method is proposed and implemented into the existing 3D CFD model named U^2RANS. In this report, the method is called the structure-embedding method (SEM), in contrast with the structure-conforming method (SCM). SCM is a traditional method in which a 3D mesh is generated to fill the fluid volume within a stream section and around structures so that the mesh "conforms" to the surface of the structures almost exactly – the reason for the term of "structure-conforming." The requirement of an accurate representation of the structure surface by the mesh is not always possible when the surface geometry is complex. Often, distorted mesh cells are created near the structure which may lead to not only the deterioration of the accuracy but also the failure of model convergence. SEM, on the other hand, relaxes the requirement of the 3D mesh to conform to the structure surface faithfully. The task of replicating the flow dynamics accurately near structure surface is achieved by the fluid dynamic solver itself, not the 3D mesh. With SEM, the no-slip flow condition at the structure surface is implemented through a special set of equations, not resolved by the 3D mesh. The approach eliminates the time-consuming and error-prone step of building a surface-conforming 3D mesh; instead a high-quality background mesh is generated for CFD modeling. The SEM method has been demonstrated to be effective in addressing the mesh generation and solver instability issues in the past (e.g., Liu 2014).

The research objective of the present study is summarized as follows: develop a stable and robust 3D CFD algorithm incorporating the IB method which is then implemented into U^2RANS. In specific, the study addresses the following research questions:

(1) Can 3D mesh generation process be simplified?

(2) Can the instability of the 3D flow solver be reduced/improved?

(3) Can the SEM method be developed in a 3D CFD model?

The benefits of the present study to Reclamation include the following, among others:

(1) Availability of a robust 3D CFD model for eco-hydraulic flow analysis with instream structures;

(2) Saving of engineers' time in carrying out a 3D CFD simulation due to the elimination of the time-consuming 3D mesh generation surface-conforming step; and

(3) Reports and papers that demonstrate the use of a 3D CFD model and provide future guidance on how to apply it.

The outcome of the present study was published in two scientific papers and they are included in the Appendix A and B in addition to this final report produced by Dr. Lai at Reclamation. This report serves as both a summary of the entire project and the documentation of the effort carried out by Reclamation engineer Dr. Yong Lai.

2. Literature Review

Instream structures are widely used at Reclamation for river restoration projects, including large wood (LW) and fish passage structures as well as fish barriers. Many projects have focused on creating flow and substrate complexity since studies have found that flow and habitat complexity is positively correlated with habitat quality (Smith et al. 2006). LW and Engineering Log Jams (ELJ's) are an effective way of creating habitat complexity for aquatic species such as salmonids and have been widely used in stream and watershed restoration projects (Pess et. al. 2012). Ecological and morphological benefits they create are well known (Abbe and Montgomery 2003). Another wide use of in-stream structures are physical and non-physical fish barriers. The migration of juvenile salmonids in the San Joaquin and Sacramento Rivers is of great environmental interest due to decline of native species. Fish diversion into the Delta may result in delayed migration, elevated risk of predation, exposure to poor water quality conditions, and mortality in pumping facilities. A recent example is the joint effort among Reclamation, California DWR, USACE and USGS on the Sacramento River (Politano et al. 2015).

Field studies may be carried out to understand flow complexity, but it can be both difficult and cost ineffective. Crowder and Diplas (2006), for example, showed that field river data often captured only the bathymetry while the large-scale roughness elements might be ignored. As an alternative, the use of computational modelling tools is gaining popularity for project applications. At present, most studies used either 1D or 2D models (Lai 2010). These low-resolution models typically adopt a global roughness value across a large area of the stream and local influence of individual rocks and large wood are not resolved properly or ignored completely. Increased computational effort has been reported by concentrating on explicitly representing individual large rocks (e.g., Lacey and Millar 2004 and Waddle 2010).

Early 3D flow models are mostly based on the hydrostatic assumption, i.e., shallow water is assumed in which the characteristic flow length scale in the vertical direction is much smaller than the characteristic length scale in the horizontal direction. These hydrostatic-assumption models are widely used in coastal and oceanic simulations; they are also popular for lake, reservoir and river modeling. For a good review, readers are referred to Lai and Wu (2019). In general, such 3D models represent an improvement over the 2D depth-averaged modeling by providing a viable way to obtain vertical distribution of important variables such as the velocity component. For 3D flows over instream structures, however, only 3D high-resolution, non-hydrostatic CFD models may offer the ultimate chance of capturing the flow complexity induced by local influences of individual rocks and LW.

3D CFD models for hydraulic engineering applications have attracted much attention in the last two decades owing to their greater versatility and accuracy. Application of 3D non-hydrostatic models has become possible owing to advances in computer technology and numerical algorithms. These models are based on the steady or unsteady Reynolds averaged Navier-Stokes (RANS) equations (they are called RANS models in this report), coupled with appropriate turbulence models. RANS models are distinguished from other 3D modeling methods such as the large eddy simulation (LES) and direct numerical simulation (DNS).

Early reported 3D models for hydraulic study include the following: Sotiropoulos and Patel (1992) developed a finite-difference model using the structured mesh. This was later modified and applied to simulate flows downstream (Sinha 1996) and upstream (Meselhe and Weber 1997) of Wanapum Dam on the Columbia River and upstream of Lower Granite Dam on the Snake River. Lai et al. (2003) developed a finite-volume unstructured mesh model that has been applied to many river engineering projects (e.g., Li et al., 2004; Weber et al. 2004). Other finite-difference, finite-volume, or finite-element RANS models have been reported such as Demuren (1993), Olsen and Melaaen (1993), Cokljat and Younis (1995), Casulli (1997), Fringer et al. (2006), etc. Most finite-difference and finite-volume 3D models used structured grids with hexahedral cells, while finite element models used unstructured grids with fixed mesh shapes (hexahedrons or tetrahedrons).

Most 3D CFD models in literature are of research nature. General-use 3D CFD models available to the public are often limited to commercial software. We will not review commercial models since their technical details are limited. Herein we review an open-source 3D CFD model: OpenFOAM - Open source Field Operation and Manipulation. OpenFOAM is a C++ toolbox for the development of customized numerical solvers for the solution of continuum mechanics problems, including computational fluid dynamics (CFD). The code is released as free and open source software under the GNU General Public License. OpenFOAM was developed by OpenCFD Ltd, maintained by the OpenFOAM Foundation (http://www.openfoam.org), and sponsored by the ESI Group, the owner of the trademark to the name OpenFOAM. The original development of OpenFOAM started at Imperial College, London. The model has been available for public use since 2004. Despite its open-source nature, OpenFOAM has been mostly limited to CFD experts. Model customization is very challenging with increasing depth into the OpenFOAM library, owing to a lack of documentation and heavy use of template metaprogramming. We could not find any theoretical papers or reports related to the CFD technologies and algorithms used by the model.

Another comprehensive 3D CFD model is VSL3D (Virtual StreamLab) developed by Professor Sotiropoulos and his colleagues (Khosronejad et al. 2014). VSL3D is a 3D flow and mobile-bed computational model capable of simulating turbulent flow and sediment transport in natural waterways with embedded and arbitrarily complex hydraulic structures. Geometric complexity is handled using the curvilinear immersed boundary (CURVIB) approach of Ge and Sotiropoulos (2007) coupled with wall modeling approach of Kang et al. (2011). VSL3D solves the unsteady Reynolds-averaged Navier-Stokes equations closed with the $k-\omega$ turbulence model. Bed material transport is simulated by solving the non-equilibrium Exner equation for the bed surface elevation coupled with a transport equation for suspended load. In their latest application (Khosronejad et al. 2014), only a single material size is used and demonstrated.

3D high-accuracy CFD modelling has been used mostly for research purpose in eco-hydraulic studies (e.g., Kang and Sotiropoulos 2012). Its popularity for practical eco-hydraulic use for restoration projects is gaining acceptance (e.g., Khosronejad et al. 2013). However, 3D CFD modeling is difficult to perform since the generation of the 3D mesh representing complex instream structures can be a daunting task. The simulation of such flows is very challenging (Carney et al. 2006). Limited reviews have been provided by, e.g., Papanicolaou et al. (2008), ASCE Sedimentation Manual (2007), and Liu and Zhang (2019), in the general area of river simulation; no review was found by the present author in the area of large wood and fish barrier modelling.

At Reclamation, the interest in large wood for river management took off in 2012 when a joint workshop was organized between Reclamation Science and Technology Office and U.S. Army Corp of Engineers (USACE). Large wood was identified as a high-priority area for inter-agency collaboration. One of the outcomes of the Workshop was the completion of the National Large Wood Manual – it provided guidelines on the assessment, planning, design, and maintenance of large wood in fluvial ecosystems (BOR and USACE 2016). 3D CFD modeling of large wood is challenging. A key bottleneck: 3D mesh generation is difficult, if not impossible, for flows with complex geometry. Severe mesh distortion may occur in order to conform the mesh to complex geometry, which can lead to instability of the CFD solver. New and novel methods are needed to overcome the above before 3D CFD models may be routinely and more widely used by engineers. A promising approach is the use of the so-called immersed boundary (IB) method (e.g., Liu 2014; Jensen et al. 2017). With IB method (called SEM), a user only needs to prepare a background 3D mesh and the surface geometry of the instream structure. The effect of the structure to flows is modeled through the special techniques within the governing equations, not the 3D mesh. For example, the IB method of Liu (2014) and Jensen et al. (2017) adopted the approach of “discrete forcing.” In this approach, an extra body force is imposed to the computational cells near the structure body. The purpose is to enforce the flow velocity on these cells to desired values such that effectively the no-slip boundary condition on the surface is honored.

3. Governing Equations

The most general governing equations for stream flows are the so-called 3D Navier-Stokes equations which represent the fundamental physical laws of mass and momentum conservation. The equation set, however, is often assemble-averaged to filter out the fluctuations due to turbulence for modeling purposes. The resultant unsteady Reynolds-Averaged Navier-Stokes (URANS) equations may be expressed as:

$$\frac{\partial U_i}{\partial x_i} = 0$$

$$\frac{\partial U_i}{\partial t} + \frac{\partial (U_i U_j)}{\partial x_j} = \frac{\partial}{\partial x_j}\left(\upsilon \frac{\partial U_i}{\partial x_j} + \tau_{ij}\right) - \frac{\partial P/\rho}{\partial x_i} + g_i$$

In the above, t is time; x_i is i-th Cartesian coordinate; ρ is water density; U_i is the mean velocity component along the Cartesian coordinate x_i; $\tau_{ij} = -\rho\overline{u_i u_j}$ is the turbulence stress with u_j the j-th turbulent fluctuating velocity component; P is mean pressure; υ is molecular viscosity of water; and g_i is the i-th component of the acceleration due to gravity.

In the above, the turbulence stress is the result of assemble averaging and representing the effect of turbulence on the fluid flow. A turbulence model is used to relate the turbulence stress tensor to other computable variables. U^2RANS adopts the two-equation model such as the standard k-ε model of Launder and Spalding (1974). That is, the Reynolds stresses is related to the mean strain rate through the turbulent eddy viscosity as:

$$\tau_{ij} = \upsilon_t\left(\frac{\partial U_i}{\partial x_j} + \frac{\partial U_j}{\partial x_i}\right) - \frac{2}{3} k\delta_{ij}$$

where δ_{ij} is the Kronecker delta and υ_t is the eddy viscosity. With the adoption of the above model, the issue now is the specification of the turbulent eddy viscosity which is computed according to the following relation:

$$\upsilon_t = C_\mu \frac{k^2}{\varepsilon}$$

where k is the turbulence kinetic energy and ε is the turbulence dissipation rate. The turbulence kinetic energy and dissipation rate are computed from their respective transport equations expressed as follows:

$$\frac{\partial k}{\partial t} + \frac{\partial (U_i k)}{\partial x_i} = \frac{\partial}{\partial x_i}\left((\upsilon + \frac{\upsilon_t}{\sigma_k})\frac{\partial k}{\partial x_i}\right) + G - \varepsilon$$

$$\frac{\partial \varepsilon}{\partial t} + \frac{\partial (U_i \varepsilon)}{\partial x_i} = \frac{\partial}{\partial x_i}\left((\upsilon + \frac{\upsilon_t}{\sigma_\varepsilon})\frac{\partial \varepsilon}{\partial x_i}\right) + C_{\varepsilon 1}\frac{\varepsilon}{k} G - C_{\varepsilon 2}\frac{\varepsilon^2}{k}$$

In the above, $G = \tau_{ij}\frac{\partial U_i}{\partial x_j}$ is the turbulence kinetic energy production rate. The standard model constants take the following values: $C_\mu = 0.09, C_{\varepsilon 1} = 1.44, C_{\varepsilon 2} = 1.92, \sigma_k = 1.0,\ \sigma_\varepsilon = 1.3$.

Common boundary conditions encountered in hydraulic flow modeling include: (a) flow inlet, (b) flow outlet, (c) solid wall, (d) plane of symmetry, and (e) free surface. Boundary conditions for the flow and turbulence variables are needed for a CFD simulation.

At a flow inlet, Cartesian velocity components or flow discharge are specified; it is implemented by specifying velocity at centers of the cell faces of the inlet. Pressure is determined by means of an extrapolation from the known values in the interior. These values of flow properties are needed in solving the flow equations (mass and momentum equations). The solution of the pressure correction equation, however, requires no pressure boundary condition because mass fluxes on these boundaries are specified and remain unchanged during the solution process. Turbulence quantities, k and ε, are user inputs at an inlet.

At a flow outlet, pressure is specified and is implemented at the centers of the cell faces while Cartesian velocity components and turbulence quantities are determined by means of an extrapolation from the values in the interior. For the pressure-correction equation, the pressure increment is set to be zero at the outlet because pressure should not change during the solution.

At solid walls, the standard wall-function approach of Launder and Spalding (1974) is used to implement the boundary condition. The log-law wall functions that incorporate the wall roughness effect are adopted. Stumpp (2001) carried out a comprehensive study using several roughness-treatment methods for river flow simulations. Results were compared to experimental data with varying surface roughness. Based on the findings of Stumpp (2001), U^2RANS adopts a specific wall-function approach described below. The wall-function may be expressed in the log-law form as:

$$\frac{u}{u_\tau} = \frac{1}{\kappa} ln\left(E\frac{u_\tau \delta}{\upsilon}\right)$$

$$u_\tau = \sqrt{\tau_w/\varrho}$$

where κ is the Von Karman constant, u_τ is the bed friction velocity, δ is the normal distance from the centroid of the first cell near a wall to the wall face and τ_w is the wall shear stress. For the turbulence quantities, the Dirichlet boundary condition is adopted for k and ε. This approach simplifies the model implementation as turbulence generation terms are not needed for the first cell touching the wall. The following turbulence quantities are implemented based on the equilibrium assumption:

$$k_B = \frac{u_\tau^2}{\sqrt{C_\mu}}$$

$$\varepsilon_B = \frac{u_\tau^3}{\kappa\delta}$$

It is noted that the U^2RANS model treats the free surface with the solid-lid assumption – i.e., the decoupled approach is adopted. The free surface is assumed known and the slip boundary condition is implemented. The solid-lid method has been widely used in 3D CFD modeling of open channel flows. It is adequate for flows with low Froude number (less than 0.2~0.5; e.g., Lai et al. 2003). The free surface input may be specified with one of two approaches: a flat surface or from the SRH-2D model results. The flat surface assumption is valid if free surface varies slowly in the flow current direction. Otherwise, surface variation may be computed using SRH-2D results. In this study, the decoupled method has been implemented as follows. The free surface elevation is first computed with SRH-2D solving the 2D depth-averaged equations. U^2RANS will then obtain the free surface elevation and form a new 3D mesh based on the elevation. The decoupled method is adequate for most open channel flows and lake/reservoir modeling. The primary limitation is that the free surface does not experience sudden vertical changes such as occurring at weirs and gates. More sophisticated free surface treatment awaits future developments. At the free surface, the velocity component normal to the surface is set to be zero while the normal derivative of the tangential velocity is zero.

The theory of the specific IB method adopted is documented in a journal paper (Appendix A) and not repeated herein.

4. Numerical Methods

The numerical solution of the above governing equations follows that reported by Lai et al. (2003). A brief description is provided below for completeness of the report.

Once a 3D mesh is available covering the model domain, the governing equations are discretized on the mesh according to the finite-volume method and cell-centered and collocated schemes. The extension to mixed cell shapes with arbitrary number of cell faces means that the CFD solver is based on most general mesh type. It facilitates the use of any mesh generation packages. In addition, the cell-centered and collocated schemes are selected so that that all flow variables are located at the centroid of a mesh cell. It is in contrast with the staggered scheme with which velocity and pressure are stored at different locations. The collocated scheme greatly simplifies the CFD solver development.

The governing equations are discretized using the finite-volume method and the Gaussian integral. The procedure was discussed by Lai et al. (2003); it is briefly presented focusing on the unsteady and implicit terms. As an illustration, consider the following general convection-diffusion equation for variable C in vector form which is a representative of all governing equations:

$$\frac{\partial C}{\partial t} + \nabla \cdot \left(\vec{V} C\right) = \nabla \cdot (\sigma \nabla C) + S_C^*$$

When all variables at time level (k-1) are given, the variables at the new time level k are solved from the following discretized equation derived by the Gaussian integration over a polygon:

$$\frac{m_0 C^k + m_1 C^{k-1} + m_2 C^{k-2}}{\Delta t} \forall + \sum_f \left(V_f^k A\right) C_f^k = \sum_f \left(\sigma_f^k A \nabla C^k \cdot \vec{n}\right) + S_C^{*k} \forall$$

In the above, Δt is time step, C^k is the variable value at time level k, $V_f^k = \left(\vec{V} \cdot \vec{n}\right)_f$ is velocity component normal to the cell face which satisfies the mass conservation, A is cell face area, $\forall$ is cell volume, C_f^k is the face value of the dependent variable, $\vec{n}$ is the cell face unit normal vector, and σ_f^k is eddy viscosity at the cell face. Summation f is over all faces of a mesh cell.

The time derivative term was added and has three parameters that determine the time discretization scheme applied. For example, $(m_0, m_1, m_2) = (1, -1, 0)$ corresponds to the first-order Euler scheme, and $(m_0, m_1, m_2) = (1.5, -2, 0.5)$ is the second-order backward differencing scheme. Note that all main variables are at time level k so that the implicit scheme is utilized to achieve model stability and robustness.

Detailed expressions for the discretized convective and diffusive terms in the above were reported in Lai et al. (2003). It is sufficient here to list the final discretized governing equation at a mesh cell (say, P); the equation is derived by linearization and expressed in a linear equation form concisely as:

$$A_P C_P = \sum_{nb} A_{nb} C_{nb} + S_C$$

In the above, C_P and C_{nb} are values of C at cell P and its neighbors; A_P and A_{nb} are the diagonal and off-diagonal matrix coefficients; and summation over "*nb*" refers to all neighboring cells connected to cell *P*. The conjugate gradient squared (CGS) solver is used to solve the above linear equation set.

The pressure-correction scheme for the collocated cell-centered method is modified from Lat et al. (2003) so that some terms are treated more accurately. First, a special procedure is adopted to compute the cell face normal velocity that is used to enforce mass conservation. Without a proper treatment, the well-known checkerboard instability, related to the velocity and pressure decoupling, may occur (Patankar 1980). In this study, the velocity-pressure coupling procedure is modified from the approach of Rhie and Chow (1983). That is, the cell face velocity is computed by averaging the momentum equation from the two cells to the cell face, leading to the following expression:

$$V_f = \langle \vec{V} \rangle \cdot \overrightarrow{n_f} - \langle \frac{\forall}{A_P} \rangle (\nabla P)_f \cdot \overrightarrow{n_f} + \langle \frac{\forall}{A_P} \nabla P \rangle \cdot \overrightarrow{n_f}$$

In the above, "< >" is the averaging operator from two cell centers to cell face, and the time level index is dropped for notation simplification. When the averaging operator is applied to a vector, it implies an application to each Cartesian component of the vector. In this study, the averaging is performed using a second-order method. The above equation shows that the mass-conserving face velocity is composed of two terms: a velocity term based on the arithmetic linear averaging, plus a correction term in the form of a 4th-order pressure damping. The pressure damping term serves to remove the spurious checkerboard instability and provides the velocity-pressure coupling.

The pressure-correction method derives the pressure-correction equation representing the mass conservation using the discretized equations. In this study, the SIMPLEC (Patankar 1980), modified for collocated scheme, is adapted for the unstructured mesh. With a known pressure field P^0 at time zero, a new velocity field may be predicted by solving the following discretized momentum equation (starred superscript denotes provisional predicted values at the new time):

$$A_P \vec{V}_P^* = H\left(\vec{V}_{nb}^*\right) - \forall \nabla P^0 + \vec{S}_V^0$$

where H stands for the linear operator $H(X) = \sum_{nb} A_{nb} X_{nb}$ and the pressure gradient term is separated from the source term. The new predicted face velocity is then computed by:

$$V_f^* = \langle \overrightarrow{V^*} \rangle \cdot \overrightarrow{n_f} - \langle \frac{\forall}{A_P} \rangle (\nabla P^0)_f \cdot \overrightarrow{n_f} + \langle \frac{\forall}{A_P} \nabla P^0 \rangle \cdot \overrightarrow{n_f}$$

Next, a corrector step is performed to compute the new pressure and velocity fields P^* and $\vec{V}_P^{**}$ such that both the continuity and momentum equations are satisfied; that is:

$$\nabla \cdot \vec{V}_P^{**} = 0$$

$$A_P \vec{V}_P^{**} = H\left(\vec{V}_{nb}^*\right) - \forall \nabla P^* + \vec{S}_V^0$$

Substitution of the incremental momentum equation into the continuity equation and application of the SIMPLEC algorithm lead to the following pressure correction equation – a Poisson equation:

$$\nabla \cdot \left(\frac{\forall}{A_p - \sum_{nb} A_{nb}} \nabla P' \right) = \nabla \cdot \vec{V}^*$$

In the above, $P' = P^* - P^0$ is the pressure correction.

For an unstructured mixed polyhedral mesh, the data structure is important. In the model development, three whole-mesh operations are implemented. The most often used is the loop over all cells. All main variables are stored at cell centroids and the linear equation solver is cell-based, so cell operation represents a major portion of the computing time. In addition, connectivity integer arrays are used to address mesh relations from a cell to its faces and neighboring cells. The second data structure is face based and created to compute the convective and diffusive fluxes. The face-based data structure requires the creation of connectivity arrays that specify the linkage from a face to its neighboring cells. The final and third is the node-based data structure, which supplies information from a mesh node to its neighboring cells. The nodal data structure is used to compute nodal values from known centroid values of a variable as well as the non-orthogonal diffusion term.

5. Mesh Generation

The present 3D CFD solver U^{2}RANS needs the generation of a 3D background mesh. There are various ways to do it, such as the *blockMesh* that comes with the OpenFOAM package. Reclamation, however, has developed its own more flexible mesh generation tool, named SRH-BGM, which is much easier to use and more flexible than *blockMesh*. The purpose and the features of the background mesh include the following: (a) The background mesh specifies the main domain and an initial set of boundaries to apply the boundary conditions; and (b) Objects, whose surface is represented with STL files, may be inserted into the background mesh so that the SEM may be adopted for CFD modeling.

3D mesh generation by SRH-BGM includes the following steps:

- A 2D horizontal mesh is generated first, which has been routinely performed by hydraulic engineers for depth-averaged 2D flow simulation.
    - At Reclamation, SMS has been used for modeling with SRH-2D and can be similarly adopted for the purpose.
- The 2D mesh includes the following information to be used by the 3D CFD modeling:
    - (a) the stream bed elevation interpolated onto the 2D mesh; and
    - (b) all the 3D vertical boundaries specified for boundary condition implementation on the 2D mesh.
- SRH-BGM is used for the semi-automatic 3D mesh generation
    - The free surface geometry is specified by the user with either the flat surface approach or from SRH-2D results.

SRH-BGM generates a 3D background mesh using the sigma-mesh approach. That is, the 3D mesh is developed by extruding the 2D mesh points vertically between the stream bed and the free surface with the equal number of vertical mesh points. The next chapter presents example cases that illustrate how the mesh is generated and used by the CFD model.

6. Model Verification and Application

Two cases are used for model verification and application herein; they are described below. For additional model verification and demonstration, the theory paper in Appendix A may be referred to.

6.1 Turbulent flow around a cylinder near scoured bed

A flume case is selected to verify that the SEM solver works well. In addition, the same case is also simulated using the SCM so that the two methods may be compared. The case is a turbulent flow around a cylinder over scoured beds. Flume experiment was carried out by Jensen et al. (1990). In the test, the flume had the size of 10 m by 0.3 m by 0.3 m. A cylinder of 3 cm diameter was placed above five scoured bed profiles and in a flowing water. The flow velocity was maintained at a constant speed of 0.2 m/s. The bed profiles represented different scour phases as observed by Mao (1986). Velocity and turbulence components were measured at various longitudinal (flow-wise) stations and the measured data may be used for comparisons with the CFD results. The same case was simulated using other CFD models in the past such as the study of Smith and Foster (2005) who used the commercial CFD model FLOW-3D.

In the present study, three bed profiles, shown in Figure 1, are selected for simulation with U^{2}RANS, corresponding to profile 1, 3 and 5. The CFD model domain is 1.1 m longitudinally along the flow direction (x), varying size vertically along the water depth direction (y), and 0.03 m laterally along the cylinder (z). At the inlet, the flow has a uniform velocity of 0.2 m/s so that the Reynolds number of the flow is 6,000 based on the approaching velocity and the cylinder diameter.

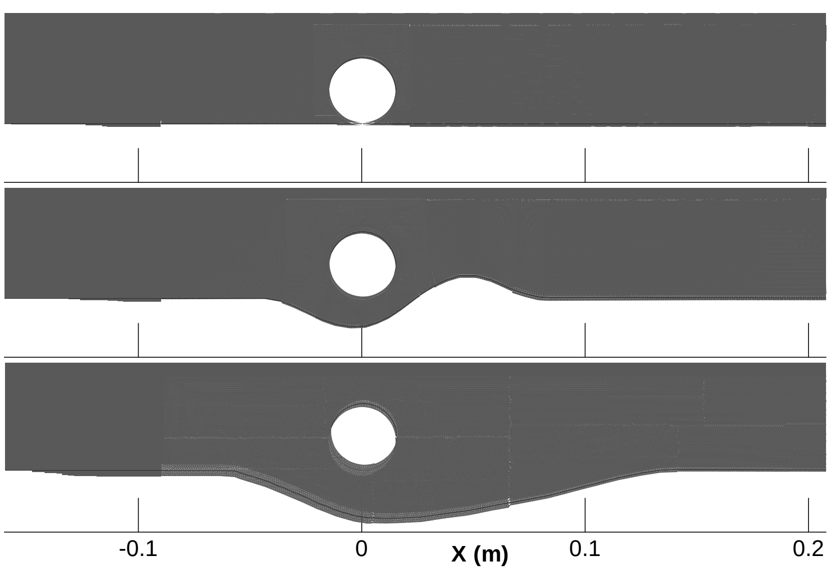

Figure 1. Three bed profiles simulated: top, middle and bottom profiles correspond to profile 1, 3 and 5, respectively, of the experiment of Jensen et al. (1990).

The SCM mesh conforms to both the cylinder and bed so that the water depth varies (approaching flow depth is 0.245 m). A closed-up view of the mesh for profile 3 is shown in Figure 2 as an example. A 2D mesh is generated first which is a combined quadrilateral and triangle cells in the x-y plane; the 3D mesh is then created by extruding the 2D mesh along the z direction. The 2D mesh has a total of 60,784 mesh cells. A much denser mesh resolution is used near the cylinder: mesh size is about 0.06 to 0.12 cm near the cylinder. With 5 cells used laterally, the 3D mesh has a total of 303,920 cells. Note that the mesh resolution is slightly finer than the finest resolution adopted by Smith and Foster (2005) to ensure that the results are almost mesh insensitive according to that study. Three meshes are generated corresponding to bed profile 1, 3 and 5, respectively, though only profile 3 mesh is discussed.

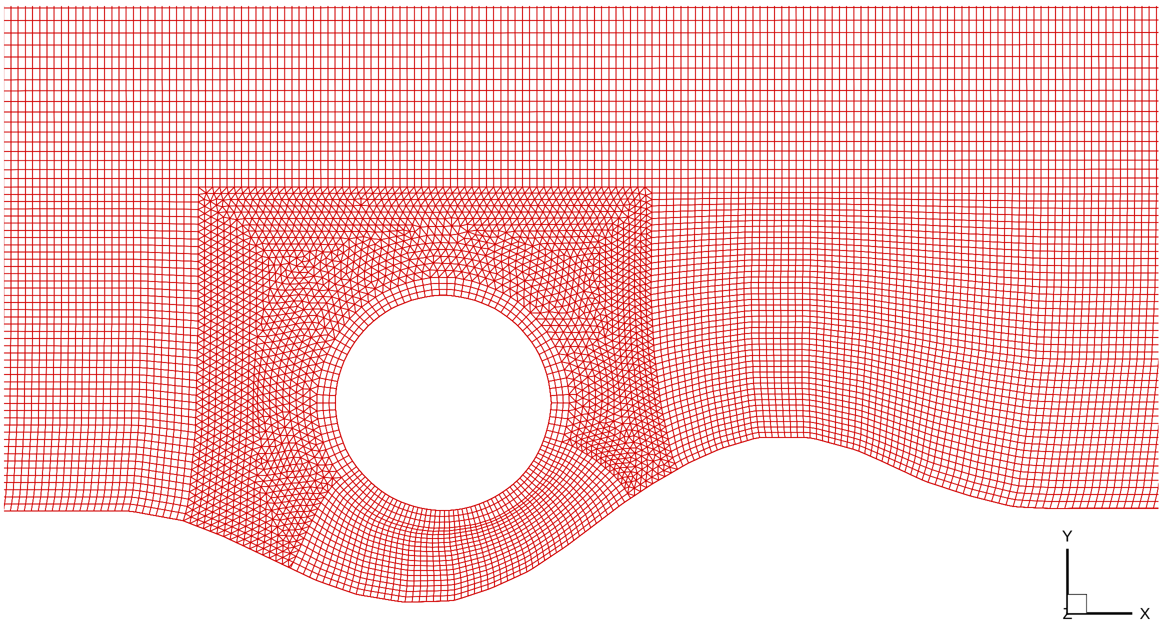

Figure 2. Terrain-conforming mesh for bed profile 3: a close-up view.

The SEM simulation needs only a background mesh which consists of rectangular mesh cells only; the model domain size is 1.1 m (x), by 0.27 m (y), by 0.03 m (z). The mesh resolution near the cylinder and scour bed is 0.1 cm which is the finest resolution used by Smith and Foster (2005). Note that only one background mesh is needed for all bed profiles as the shape of the cylinder and scour bed profiles are embedded into the background mesh and automatically processed by the CFD model. A close-up view of the fluid and IB mesh cells is shown in Figure 3 after the cylinder and bed profile 3 geometry is embedded into the background mesh. The meshes for the two other profiles are similar.

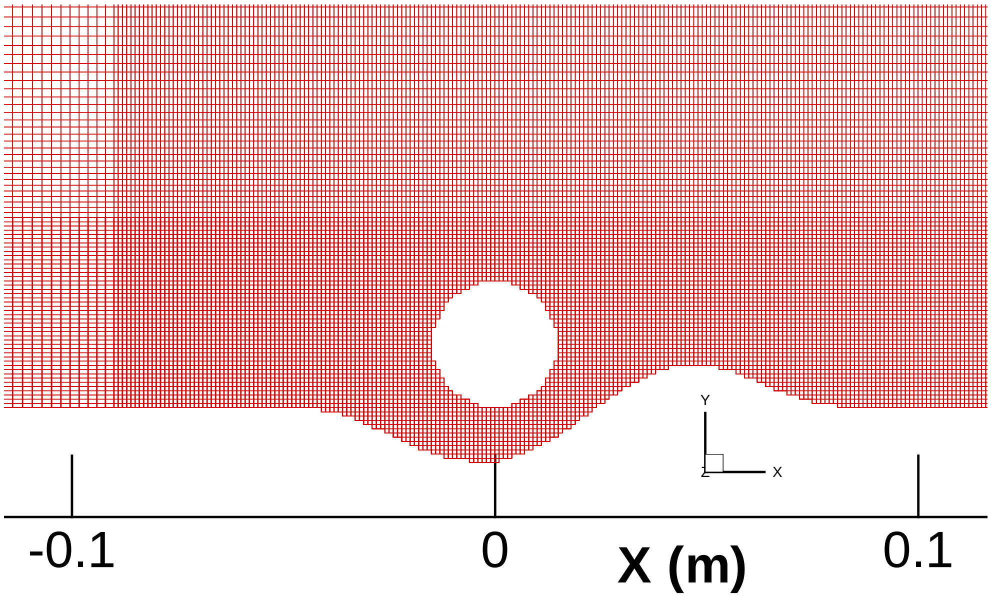

Figure 3. The fluid and IB mesh cells of the background mesh used in the terrain-embedding CFD modeling after the cylinder and scour bed geometry inserted.

Both SCM and SEM are used to simulate the case with the three bed profiles (1, 3 and 5). The CFD results are compared with each other and against the flume measured velocity data. These results are presented below to shed light on the two CFD methods.

The overall flow patterns for the three profiles are shown in Figure 4. The flow patterns are varying drastically with the changing bed profiles. A noteworthy feature is that the CFD results show that unsteady vortex shedding starts to develop with profile 5, while flows with profiles
1 and 3 remain steady. This result is consistent with the findings of Smith and Foster (2005).

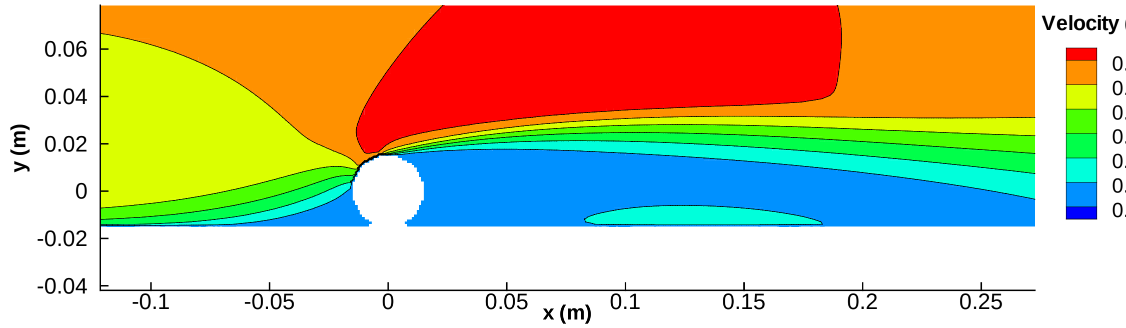

(a) Profile 1

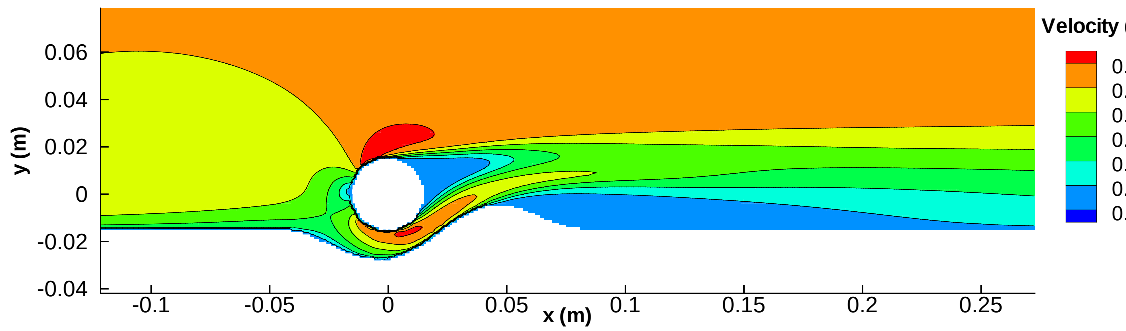

(b) Profile 3

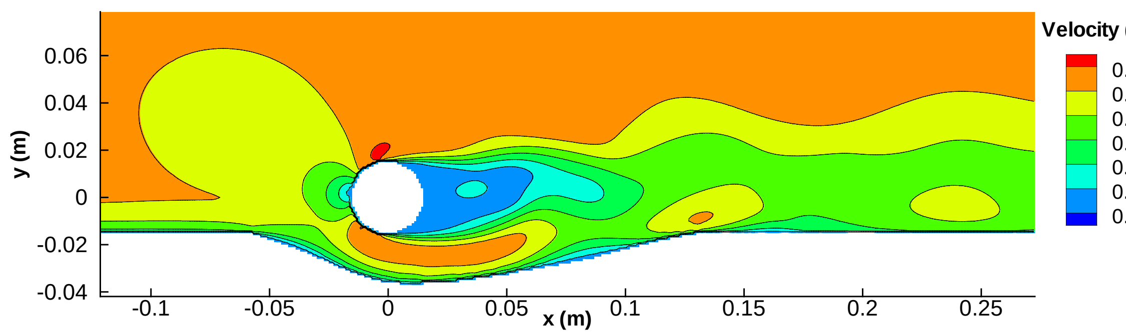

(c) Profile 5

Figure 4. CFD predicted velocity magnitude contours of the flow pattern with the terrain-embedding method.

The streamwise velocity component is compared in Figure 5 between CFD results and measured data. The flow approaches the cylinder with a near-logarithmic velocity profile with all cases and the CFD results agree with the measured data well. The impact of the cylinder is still significant even at the last measured station eight cylinder-diameters downstream (x=24 cm). The embedding CFD results agree with the measured data reasonably well for all three profiles and eight streamwise stations. The conforming CFD results agree also in most stations except for the three stations downstream of the cylinder for profile 3. SCM predicted a stronger flow near the bed downstream of the cylinder than the data, which significantly shortens the flow reversal in the zone. The mismatch is primarily caused by the inability of the model to resolve the ending of the jet and beginning of the flow separation on the upper and lower portions of the cylinder, leading to a different wake characteristic. It is unclear why the SEM CFD predicts the wake dynamics of profile 3 better than the SCM. Probable causes may be due to the use of different wall functions as well as the different implementations of the wall-function. Wall-function will influence the predicted boundary layer as well as the separation locations. It is noted that the results obtained by Smith and Foster (2005) with FLOW-3D are similar to our results of the SCM modeling for profile 3.

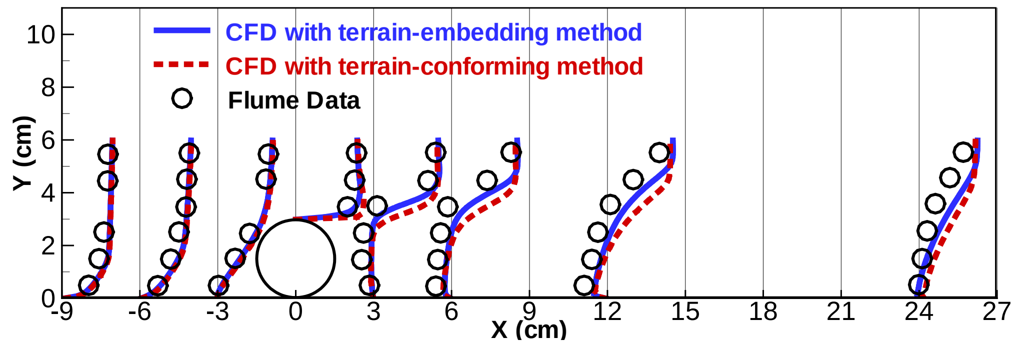

(a) Profile 1

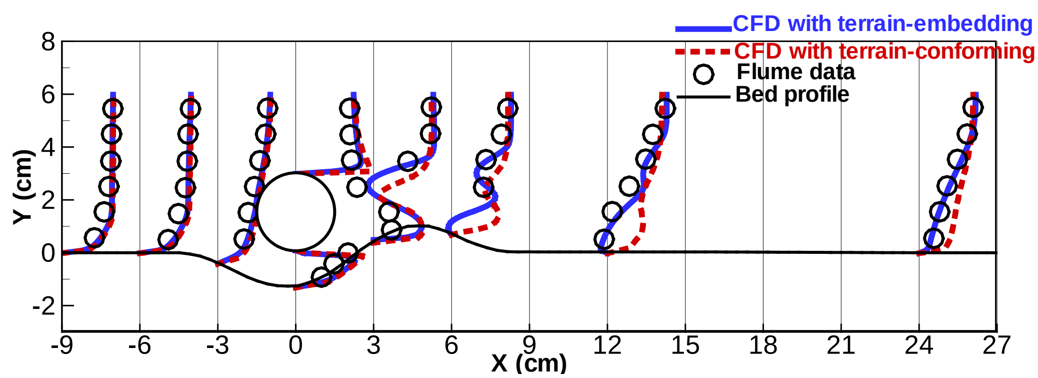

(b) Profile 3

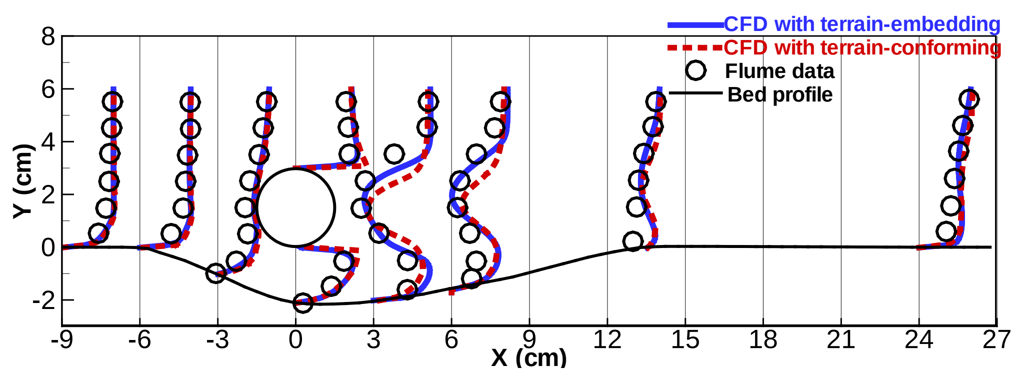

(c) Profile 5

Figure 5. Comparison of CFD and measured streamwise velocity components (U) along eight streamwise stations. Scaling of U is such as one unknit of X is 10 cm/s.

The above flume case is used to compare the SEM and SCM CFD modeling. It is found that SEM works well for the simulated case: (a) the mesh generation process is relatively simple; (b) the numerical simulation is stable; (c) the computing time is reduced as it was found that the convergence was faster than the SCM; and (d) the simulated results are good in comparison with the measured data.

The study shows that the SEM of U^2RANS has a great potential to be used for practical stream flow modeling with complex terrains. The greatest benefit of the method, compared with the traditional SCM, is that the mesh generation is much simplified, and the good mesh quality may be maintained. These benefits point to the potential of SEM for predicting scour processes when the mesh of the scoured bed is moving – a future development direction. In such moving-mesh applications, SCM is known prone to numerical instability and degradation of model accuracy. SEM, however, will be expected to perform well, which will be our future research and development effort.

6.2 Flow through a 6-Piece Engineered Log Jam

A complex flow through a six-piece Engineered Log Jam (ELJ) is simulated and validated. The case has experimental study results for comparison.

6.2.1 Experimental Test

An experiment has been carried out providing the data for CFD model validation. The 6-piece ELJ in Figure 6 is installed in the Cognitive Ecology and Ecohydrology Research Flume (CEERF) at the Engineer Research and Development Center, US Army Corps of Engineers, Vicksburg, MS. It is a recirculating-type flume and the layout is shown in Figure 7. The test section of the flume has the dimensions of 2.434 m (8 ft) in width, 1.372 m (4.5 ft) in height, and 9.754 m (32 ft) for the straight test section. The measurement facility is equipped to measure velocity around ELJ in a controlled laboratory setting. Velocity is measured with a Nortek Vectrino+ Velocimeter. During velocity measurements, changes are made to the configuration settings depending on proximity to woody debris, depth, and water turbulence. Sampling rate is constant at 50 Hz and data are collected at each point for 1.5-2 minutes. Raw data are filtered in WinADV32 (Version 2.031) using phase-space threshold despiking. Multiple flume runs are planned using different pump rates to generate different flows. The specific case reported corresponds to the pump rate of 15 Hz which produces an approximate mean flow velocity of 0.25 m/s in the test section. Velocity was measured at 3-10 different vertical depths (z-axis).

(a) A photo of the 6-piece ELJ (b) The STL Object of the ELJ

Figure 6. The 6-piece ELJ scanned and developed into an STL object.

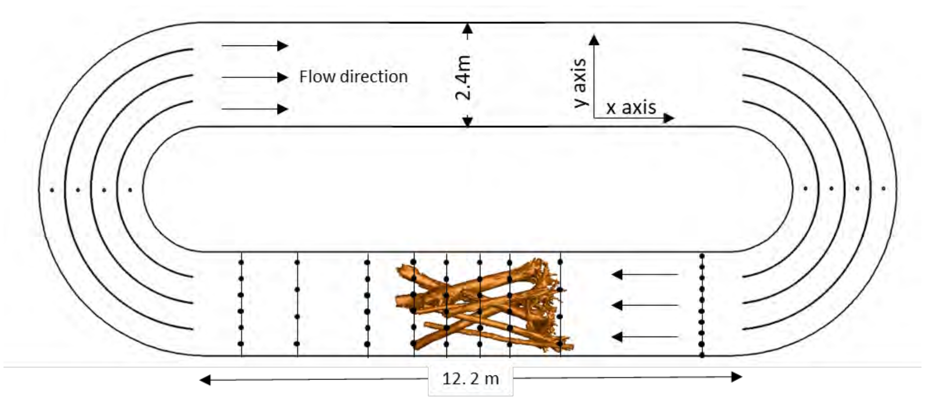

Figure 7. Layout of the flume, test section and ELJ; black circles are the measuring points.

6.2.2 Mesh and ELJ Representation

The CFD model domain selected is the test section of the flume, along with a slight extension of the upstream and downstream boundaries to minimize boundary conditions. The model domain has a length of 12.192 m (40 ft) in the flow direction, a width of 2.434 m (8 ft), and a depth of 1.070 m (3.51 ft). A 2D mesh for the rectangular domain is easily generated by SMS, consisting of 24,925 mixed triangle-quadrilateral cells. The 3D background mesh is easily generated using SRH-BGM: a sigma mesh by extruding the 2D mesh vertically with 47 cells. The total number of cells of the background mesh is 1,171,475 cells. The bed elevation is 0 and the surface elevation is 1.07p m (3.51).

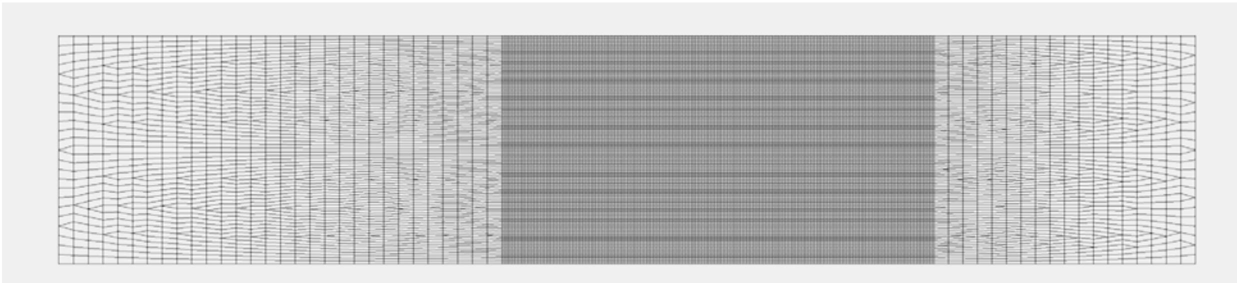

Figure 8. The 2D mesh overview.

The ELJ is constructed from six pieces of large woods harvested locally and an experiment is carried out at the Engineer Research and Development Center, US Army Corps of Engineers, Vicksburg, MS. The woods are anchored together so that it may be lifted and placed in the flume (see Figure 6a).

A stationary terrestrial LiDAR scanner is used to capture the ELJ surface which creates a high-resolution point cloud data set. The raw 3D point cloud is downloaded and then imported into a CAD software to develop a solid model representing the ELJ surface. The point cloud is edited and processed for solid modeling. Multiple CAD software packages may be used. In this study, the post-processing survey software of Trimble Realworks is used for scan registration and initial editing, and 3D Systems Geomatic software (Geomagic) is used to develop a watertight solid. Figure 6b shows the STL object used for the mesh generation.

6.2.3. Results and Discussion

CFD simulation is carried out using the 3D background mesh, the ELJ scanned and saved as STL format, and the SEM method. The boundary conditions are as follows: an average upstream velocity of 0.25 m/s is imposed corresponding to the experiment data; zero pressure (constant water surface elevation) is assumed along the exit boundary; free surface is handled with the solid-lid assumption; and the rest of the boundaries (flume bed and front and back surfaces) are treated as the no-slip walls. In addition, the turbulence is closed with the two-equation k-ε model.

The steady-state solution starts from a constant flow (0.25 m/s) and constant pressure (0 Pa). The predicted velocity field is graphically displayed in Figure 9, providing an overview of the flow through the ELJ. The results visually match the flow field observed in the flume. It is seen that the presence of the ELJ creates a significant blockage to the flow. Water is pushed away from the ELJ towards the two banks (side walls), creating a much larger velocity near the banks than the average velocity (as large as 0.65 m/s). A large wake is generated behind the ELJ and extends downstream all the way to the computational domain exit.

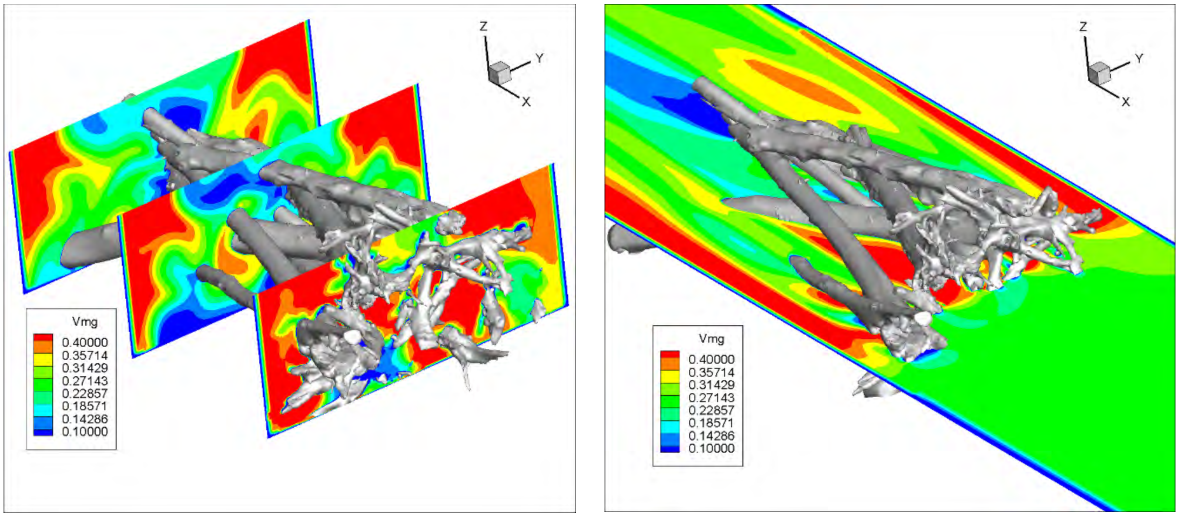

(a) Three X cross-sections (b) Cross-section with Z=0.549 m (1.8 ft)

Figure 9. Predicted velocity distributions on cutting planes.

CFD results are compared with the measured data in the graphical form. Figure 10 compares the water surface elevation. The water surface elevation of the CFD model is computed using the equation $\eta = \eta_0 + P/(\rho g)$, where η_0 is the elevation at the exit, P is surface pressure, ρ is water density, and g is the gravity constant. The relation is based on the solid-lid method assumption, which was found adequate for relatively low Froude number flows (Lai et al. 2003). For the present cae, the Froude number is 0.08. The agreement between CFD and experiment is qualitatively good considering that the contours of the measured elevation are generated from a relatively scarce set of measured points. The CFD predicted velocity vector near the water surface is further compared with the measured data in Figure 11. Again, CFD results agree with the experiment qualitatively.

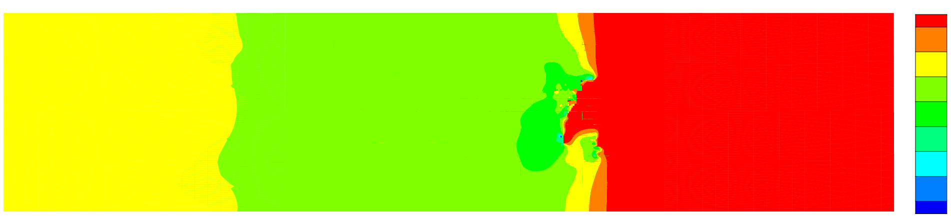

(a) CFD Result

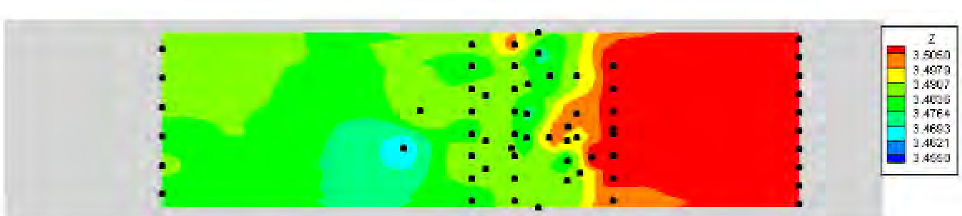

(b) Experimental Data

Figure 10. Comparison of CFD and experimental data of water surface elevation (note that measured zone is a smaller subset of the CFD model domain).

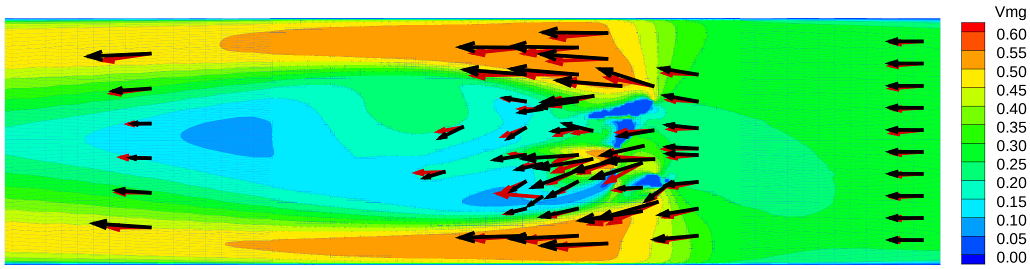

Figure 11. Comparison of predicted (red) and measured (black) velocity vector near the water surface (background contours are the CFD predicted surface velocity magnitude).

7. Concluding Remarks

In this research, a special IB method based on the SEM concept is developed and implemented into U^2RANS in collaboration with multiple partners, in particular, Prof. Xiaofeng Liu at the Penn State University, and David Smith at the U.S. Army Corp of Engineers (USACE).

The CFD modeling procedure is proposed so that 3D CFD modeling of flows through complex instream structures may be carried out for ecohydraulic projects. All components of a CFD package to perform the CFD modeling are described. The new capability is described and verified using selected benchmark cases at the Penn State University. The model is further checked, modified and tested at Reclamation. In specific, a turbulent flow around a cylinder near scoured bed is used to test and validate the model. Further, a complex flow through a 6-piece ELJ is used to demonstrate that the model works for complex flows. The ELJ case is further constructed and lab-tested by the collaborator at USACE. The experimental data are used to validate the model further.

Finally, the research results have been documented by scientific papers in addition to the project report (See Appendix A and B).

Future continued research and development are needed to advance the model further so that the model can be more practical for project applications. They include the following:

(a) Local mesh refinement needs to be developed as only one background mesh is adopted without the local mesh refinement capability;

(b) The ability of the model to predict bed shear stress is to be checked; most probably, the current approach needs to be improved;

(c) Sediment transport modeling capability with SEM is to be developed once the shear stress accuracy is improved and validated;

(d) New free surface simulation method is to be developed such as the Volume of Fluid (VOF) method; and

(e) Parallelization of the model is important in practical applications.

References

Abbe, T.B. and Montgomery, D.R. (2003). Patterns and processes of wood accumulation in the Queets River basin, Washington. Geomorphology 51:81–107.

ASCE (2007). ASCE Sedimentation Manual. Sedimentation Engineering: Processes, Measurements, Modeling and Practice. ASCE Manual and Reports on Engineering Practice No.110. Reston, VA. Marcelo Garcia (ed).

Carney, S.K., Bledsoe, B.P., and Gessler, D. (2006). Representing the bed roughness of coarse-grained streams in computational fluid dynamics. Earth Surface Processes and Landforms, 31(6), 736-749.

Casulli, V. (1997). Numerical simulation of three-dimensional free surface flow in isopycnal coordinates. Int. J. Numer. Methods Fluids, 25, 645–658.

Cokljat, D., and Younis, B. A. (1995). Second-order closure study of open-channel flows. J. Hydraul. Eng., 121~21, 94–107.

Crowder, D. W. and Diplas, P. (2006). Applying spatial hydraulic principles to quantify stream habitat. River Research and Applications, 22(1), 79-89.

Demuren, A. O. (1993). A numerical model for flow in meandering channels with natural bed topography. Water Resour. Res., 19(4),1269–1277.

Fringer, O.B., Gerritsen, M., and Street, R.L. (2006). An unstructured-grid, finite-volume, nonhydrostatic, parallel coastal ocean simulator. Ocean Modeling, 14(3-4):139–173.

Ge, L., and Sotiropoulos, F. (2007). A numerical method for solving the 3D unsteady incompressible navierstokes equations in curvilinear domains with complex immersed boundaries. J. Comput. Phys., 225(2), 1782–1809.

Jensen, B. L., Sumer, B. M., Jensen, H. R., and Fredsoe, J. (1990). Flow around and forces on a pipeline near a scoured bed in steady current. Journal of Offshore Mechanics and Arctic Engineering, 112(3), 206-213.

Jensen, B.L., Liu, X., Christensen, E. D., and Rønby, J. (2017). Porous Media and Immersed Boundary Hybrid-Modelling for Simulating Flow in Stone Cover-Layers. Paper presented at Coastal Dynamics 2017, Helsingør, Denmark.

Kang, S., Lightbody, A., Hill, C., and Sotiropoulos, F. (2011). High resolution numerical simulation of turbulence in natural waterways. Adv. Water Resour., 34(1), 98–113.

Kang, S. and Sotiropoulos, F. (2012). Numerical modeling of 3D turbulent free surface flow in natural waterways. Advances in Water Resources, Volume: 40, Pages: 23-36, DOI:10.1016/j.advwatres.2012.01.012.

Khosronejad, A., Hill, C., Kang, S., and Sotiropoulos, F. (2013). Computational and experimental investigation of scour past laboratory models of stream restoration rock structures, Advances in Water Resources, Volume 54, 2013, Pages 191-207, ISSN 0309-1708, https://doi.org/10.1016/j.advwatres.2013.01.008.

Khosronejad, A, Kozarek, J.L., and Sotiropoulos, F. (2014). Simulation-Based Approach for Stream Restoration Structure Design: Model Development and Validation. J. Hydraul. Eng., 140, (ASCE)0733-9429/04014042.

Lacey, R.W.J. and Millar, R.G. (2004). Reach scale hydraulic assessment of instream salmonid habitat restoration. Journal of the American Water Resources Association, 40(6),1631-1644.

Lai, Y.G., Weber, L.J. and Patel, V. C. (2003). Nonhydrostatic three dimensional method for hydraulic flow simulation. I: Formulation and verification. J. Hydraul. Eng., 129(3), 196–205.

Lai, Y.G. (2010). Two-Dimensional Depth-Averaged Flow Modeling with an Unstructured Hybrid Mesh. J. Hydraulic Engineering, ASCE, 136(1), 12-23.

Lai, Y.G. and Bandrowski, D.J. (2014). Large Wood Flow Hydraulics: a 3D Modelling Approach. Proc. 7th International Congress on Environmental Modelling and Software, International Environmental Modelling and Software Society, San Diego, California, USA, D.P. Ames, N. Quinn (Eds.).

Lai, Y.G. and Wu, K. (2019). A Three-Dimensional Flow and Sediment Transport Model for Free-Surface Open Channel Flows on Unstructured Flexible Meshes. Fluids 2019, 4, 18; doi:10.3390/fluids4010018.

Launder, B.E., and Spalding, D.B. (1974). The numerical computation of turbulent flows. Comput. Methods Appl. Mech. Eng., 3, 269–289.

Li, S., Lai, Y.G., Weber, L.J., Silva, J.M., Patel, V.C., (2004). Validation of a Three-Dimensional Numerical Model for Water-Pump Intakes. J. Hydraulic Research, IAHS, vol.42(3).

Liu, X. (2014). A new immersed boundary method for simulating free-surface flows around arbitrary objects. In Proceedings of the International Conference on Fluvial Hydraulics, RIVER FLOW 2014 (pp. 141-146). (Proceedings of the International Conference on Fluvial Hydraulics, RIVER FLOW 2014). CRC Press/Balkema. https://doi.org/10.1201/b17133-24.

Liu, X. and Zhang, J. (editors) (2019). Computational Fluid Dynamics: Applications in Water, Wastewater, and Stormwater Treatment. ASCE Publications, 2019. https://doi.org/10.1061/9780784415313

Mao, Y. (1986). The interaction between a pipeline and an erodible bed. PhD thesis, Technical Univ. of Denmark, Lyngby, Denmark.

Meselhe, E. A., and Weber, L. J. (1997). Validation of a three dimensional model using field measurements in a large scale river reach. Proc., 27th Congress of the IAHR, Theme B, Vol. 2, pp. 827–832.

Olsen, N., and Melaaen, C. (1993). Three-dimensional calculation of scour around cylinders. J. Hydraul. Eng., 10.1061/(ASCE)0733-9429(1993)119:9(1048), 1048–1054.

Papanicolaou, A.N.T., Elhakeem, M., Krallis, G., Prakash, S., Edinger, J. (2008). Sediment Transport Modeling Review - Current and Future Developments. J. Hydraulic Engineering, ASCE, 134(1), 1-14.

Patankar, S. V. (1980). Numerical heat transfer and fluid flow, McGraw-Hill, New York.

Pess, G.R., Liermann, M.C., McHenry, M.L., Peters, R.J., and Bennett, T.R. (2012). Juvenile Salmon Response to the Placement of Engineered Log Jams (ELJs) in the Elwha River, Washington State, USA. River Res. Applic., 28: 872–881. doi: 10.1002/rra.1481

Politano, M., Martin, E., Lai, Y.G., Bender, M., and Smith, D.L. (2015). Modeling of a non-physical fish barrier. 10th Federal Interagency Sedimentation Conference, April 19-23, 2015, Reno, Nevada

Rhie, C. M., and Chow, W. L. (1983). umerical study of the turbulent flow past an airfoil with trailing edge separation. AIAA J., 21(11),1526–1532.

Sinha, S. K. (1996). Three-dimensional numerical model for turbulent flows through natural river reaches. PhD thesis, Civil and Environmental Engineering, The University of Iowa, Iowa.

Smith, D.L., Brannon, E.L., Shafii, B., and Odeh, M. (2006). Use of the average and fluctuating velocity components for estimation of volitional rainbow trout density. Transactions of the American Fisheries Society, 135(2), 431-441.

Smith, H. D. and Foster, D. L. (2005). Modeling of flow around a cylinder over a scoured bed. Journal of waterway, port, coastal, and ocean engineering, 131(1), 14-24.

Sotiropoulos, F., and Patel, V. C. (1992). Flow in curved ducts of varying cross section. IIHR Report No. 358, Iowa Institute of Hydraulic Research, The University of Iowa, Iowa City, Iowa.

Stumpp, S. (2001). Investigations on Modeling of Large River-Bed Roughness, M.S. Thesis, University of Stuttgart and IIHR.

USBR and USACE (Bureau of Reclamation and U.S. Army Engineer Research and Development Center). (2016). National Large Wood Manual: Assessment, Planning, Design, and Maintenance of Large Wood in Fluvial Ecosystems: Restoring Process, Function, and Structure.

Waddle, T. (2010). Field evaluation of a two-dimensional hydrodynamic model near boulders for habitat calculation. River Research and Applications, 26(6), 730-741.

Weber, L.J., Huang, H., Lai, Y.G., and McCoy, A., (2004). Modeling Total Dissolved Gas Production and Transport Downstream of Spillways – Three-Dimensional Model Development and Applications. Int. J. River Basin Management, vol.2(3), 157-167.

Appendix A. SEM Theory Paper

An improved immersed boundary method for simulating flow hydrodynamics in streams with complex terrains

Yalan Song[1], Yong G. Lai[2] and Xiaofeng Liu[3]

1 Department of Civil and Environment Engineering, Pennsylvania State University, University Park, PA 16802; yxs275@psu.edu
2 Technical Service Center, U.S. Bureau of Reclamation, P.O. Box 25007, Denver, CO 80225; ylai@usbr.gov
3 Department of Civil and Environment Engineering, Institute of Computational and Data Sciences, Pennsylvania State University, University Park, PA 16802; xzl123@psu.edu

Abstract

Three-dimensional (3D) computational fluid dynamic (CFD) simulations gain substantial popularity in recent years for stream flow modelling. The complex terrain in streams is usually represented by a 3D mesh conforming to the terrain geometry. Such terrain-conforming meshes are time-consuming to generate. In this work, an immersed boundary method is developed in an existing terrain-conforming CFD model named U2RANS as an alternative, in which terrains are represented implicitly in the Cartesian background mesh. An improved two-layer wall function is proposed in the framework of the $k-\varepsilon$ turbulence model, with the aim of producing accurate and smooth wall shear stress distribution and paving the way for future model development on sediment transport and scour modeling. The improvement overcomes the inherent discontinuity and nonlinearity of the two-layer velocity profile, which causes error in the estimation of shear velocity. The new algorithm utilizes a distance control on the image point in immersed boundary method and a modification of velocity prediction in the laminar layer. The improved immersed boundary method is tested with 1D, 2D, and 3D cases, and comparisons with flume experiments show promising results.

1. Introduction

Traditional three-dimensional (3D) modeling requires a 3D mesh to conform to domain geometry – termed terrain-conforming method in this paper. Despite the widespread use of terrain-conforming method in Computational Fluid Dynamics (CFD) models, generation of a high-quality mesh is still a challenging task in 3D modeling of flows over complex terrain. A very refined near-wall mesh must be used to resolve the boundary layer to produce an accurate solution. The stability and accuracy of the terrain-conforming method highly depend on the mesh quality. In addition, the mesh size increases rapidly with the increase of Reynolds numbers (Mittal and Iaccarino, 2005).

In this work, we aim to present a user-friendly 3D CFD model for practical applications in hydraulic engineering. An alternative way to the terrain-conforming method is the immersed boundary (IB) method, in which terrains are embedded in a background mesh. The boundary conditions on terrain surface are implicitly represented by modifying the governing equations of the flow. Such a method is also referred to as the terrain-embedding method in this work. Special numerical treatments are developed to implement the solid boundary conditions for turbulent flows near complex terrain and solid object. For example, a discrete-forcing term can be added in the discretized Navier-Stokes equations to represent the embedded terrain (Mohd-Yosuf, 1997; Verzicco et al., 1998). With the IB method, mesh generation becomes relatively simple as only a background mesh is needed, and mesh quality is easy to control. A key issue of the IB method is the model accuracy in simulating turbulent flows although it has been demonstrated for laminar flows. Another advantage of the IB method is that it can easily track terrain deformation, which is important in the simulation of sediment transport and scour. With the terrain-conforming methods, the mesh has to be regenerated to conform to the terrain or solid body movement in each morphological time step. The mesh regeneration is difficult to perform and may lead to numerical instability and loss of accuracy due to the deterioration of the mesh quality caused by large movement. With the IB method, terrain deformation is captured by recalculating the discrete-forcing term and no mesh changes are necessary.

A key variable in sediment transport and scour simulation is the wall shear stress on erodible bed. Existing algorithms of the IB method have demonstrated good performance in the prediction of flow velocity (Kim et al., 2001; Tessicini et al., 2002). However, the accuracy and smoothness of the wall shear stress in the IB method need improvements. This issue is mainly caused by the poor prediction of the velocity profile between the near-wall cell and the terrain boundary. The other reason is the mass conservation problem on the terrain boundary (Harada et al., 2016). In addition, the implementation of a wall function in the IB method is a significant challenge, especially for high Reynolds number flows. To avoid high mesh resolution in the near-wall region, attempts have been made in the implementation of wall models in the large eddy simulation (LES) framework (Roman et al. 2009; Yang et al. 2015). For example, Roman et al. (2009) proposed a RANS-like (Reynolds-Averaged Navier-Stokes-like) eddy viscosity to reconstruct the wall shear stress in LES.

Considering that there are drastically different time scales in hydrodynamics and morphodynamics (the latter is much slower than the former) (Termini, 2011), a wall model in the RANS framework is more suitable for real-world applications. Tamaki et al. (2017) proposed a Spalart-Allmaras (SA) wall model using the IB method, and modified the eddy viscosity to balance the shear stress. Capizzano (2011) adopted a two-layer wall model in the near-wall region for $k-\omega$ and $k-g$ turbulence models with a blending estimation of ω and g. Zhou (2017) applied a blending of Spalding's law, Reichardt's law, and log-law in the SST $k-\omega$ turbulence model. The key of the most existing wall functions is to avoid the transition of the wall model between the viscous sublayer and the log-law sublayer by either using the blending turbulence variables or using continuous velocity profiles.

Despite the progresses made in the IB methodology and its applications in river hydraulics, mature models are yet to be developed to have the accuracy, stability, and efficiency needed for real-world applications. In particular, a reliable sediment transport and scour model would hinge on the accurate prediction of the bed shear stress. In this work, we present an improved IB algorithm which is then implemented into the terrain-conforming model of Lai et al. (2003) (named U^2RANS). The aim is to develop an IB-method based 3D model so that accurate flow and bed shear stress may be predicted. This paper extends the work presented in Lai (2020) and Song et al. (2020). Specifically, a two-layer wall function is implemented in association with the $k-\varepsilon$ turbulence model (Lauder et al., 1983) and the IB method. The model is then verified to produce accurate velocity field as well as a smooth and accurate wall shear stress distribution. A key contribution of the present study is the improvement of the model accuracy through the control of the image point position, which is a point used in the IB model to reconstruct the near-wall flow field. In addition, a modification of the wall model in the viscous sublayer allows better handling of the discontinuity between the viscous sublayer and the logarithmic layer. As a result, a better estimation of wall shear stress can be achieved.

The new IB-method based U²RANS model is validated and demonstrated using a number of flow cases in the following. As discussed before, due to the limitations of the terrain-conforming method, the terrain-embedding method is more suitable for modeling of real-world cases, in particular, for sediment transport and scour modeling. The scour modeling is under development and will be reported in the future.

2. Numerical Model

U²RANS is a 3D CFD model using the unstructured mesh with arbitrarily shaped cells (Lai et al., 2003). The flow is assumed incompressible, viscous, and Newtonian. The governing RANS equations are as follows:

$$\nabla \cdot \boldsymbol{U} = 0 \tag{1}$$

$$\frac{\partial \boldsymbol{U}}{\partial t} + (\mathbf{U} \cdot \nabla)\boldsymbol{U} = \upsilon \nabla^2 \boldsymbol{U} + \nabla \cdot \tau - \frac{\nabla P}{\rho} + \boldsymbol{g} \tag{2}$$

where t is time; ρ is the flow density; $\boldsymbol{U}$ is the mean velocity; $\boldsymbol{\tau}$ is the turbulence stress; P is the mean pressure; υ is the kinematic viscosity; and $\boldsymbol{g}$ is the gravity acceleration.

The Reynolds stress tensor $\boldsymbol{\tau}$ is calculated with the standard k-ε model of Launder and Spalding (1974):

$$\boldsymbol{\tau} = \upsilon_t(\nabla \boldsymbol{U} + (\nabla \boldsymbol{U})^{\mathrm{T}}) - \frac{2}{3}k\boldsymbol{\delta} \tag{3}$$

where $\boldsymbol{\delta}$ is the Kronecker delta (a unit tensor) and the eddy viscosity υ_t is calculated as:

$$\upsilon_t = C_\mu \frac{k^2}{\varepsilon} \tag{4}$$

where $C_\mu = 0.09$; k is the turbulence kinetic energy; and ε is the turbulence dissipation rate.

The transport equations for k and ε are:

$$\frac{\partial k}{\partial t} + \nabla \cdot (k\boldsymbol{U}) = \nabla \cdot \left(\left(\upsilon + \frac{\upsilon_t}{\sigma_k} \right) \nabla k \right) + G - \varepsilon \tag{5}$$

$$\frac{\partial \varepsilon}{\partial t} + \nabla \cdot (\varepsilon \boldsymbol{U}) = \nabla \cdot \left(\left(\upsilon + \frac{\upsilon_t}{\sigma_\varepsilon} \right) \nabla \varepsilon \right) + C_{\varepsilon 1}\frac{\varepsilon}{k}G - C_{\varepsilon 2}\frac{\varepsilon^2}{k} \tag{6}$$

where $G = \boldsymbol{\tau}{:}\nabla \boldsymbol{U}$ is the turbulence generation rate; $C_{\varepsilon 1} = 1.44$; $C_{\varepsilon 2} = 1.92$; $\sigma_k = 1.0$; and $\sigma_\varepsilon = 1.3$.

Numerical solution of the above flow equations involves the use of a mesh to cover the model domain and then discretization of the governing equations. With the IB method, only a background mesh is needed. The background mesh itself, however, can be unstructured and assume polyhedral shapes. Such a mesh is the most flexible and has the advantage of uniting various mesh topologies into a single formulation. The cell-centered scheme is adopted with all dependent variables located at the centroid of a mesh cell. The other alternatives include the cell-vertex scheme with which all variables are at cell's vertices or staggered scheme with which velocity and pressure are stored at difference locations. The governing equations are discretized using the finite-volume approach using the Gauss theorem. An advantage of the finite-volume method is that the conservation of any flow property can be achieved locally and globally. The detailed numerical method was referred to Lai et al. (2003) and not repeated herein.

3. Immersed boundary implementation

The proposed IB method uses a discrete forcing approach where the forcing term is cell-based for an unstructured mesh. The IB cells are the cells cut by the immersed surface, and their cell centers are located on the fluid side (yellow cells shown in Fig. 1). Three different points are identified: 1) IB cell center (IB); 2) hit point (HP) which is the intersection of the immersed surface with its normal line through the cell center; 3) image point (IP) which is the point on the extended line of the normal vector through the cell center in the fluid field. Three different characteristic lengths are identified: 1) wall distance y_{IB}: the distance from the IB cell center to the corresponding hit point; 2) image distance y_{IP}: the distance from the image point to the corresponding hit point; 3) IB cell length l_*: the minimum dimension of all IB cells. To enforce the turbulence model conditions at the IB cell centers, the following steps are carried out:

1) The flow velocity U_{IP} at an image point is reconstructed by using a distance-based weighting procedure with the neighboring cells around the image point.

2) Based on the log-law velocity profile, the dimensionless distance y_{IB}^+ and y_{IP}^+ are computed (iteratively) as:

$$y_{IP,n+1}^+ = \frac{y_{IP,n}^+ + \frac{\kappa U_{IP} y_{IP}}{\upsilon}}{1 + \ln\left(E y_{IP,n}^+\right)}; \quad y_{IB}^+ = y_{IP}^+ \frac{y_{IB}}{y_{IP}} \tag{7}$$

where $E = 9.8$ and $\kappa = 0.41$.

3) The shear velocity u_τ on the immersed surface is calculated as:

$$u_\tau = \frac{y_{IP}^+ \upsilon}{y} \tag{8}$$

4) The flow velocity U_{IB}, k_{IB}, and ε_{IB} at the IB cell center are calculated based on y_{IB}^+:

$$U_{IB}^{new} = U_{IP} - \frac{1}{\kappa} u_\tau \log\left(\frac{y_{IP}}{y_{IB}}\right) \tag{9}$$

$$k_{IB} = \frac{C_k \log(y_{IB}^+)}{\kappa} + B_k \tag{10}$$

$$\varepsilon_{IB} = \frac{C_\mu^{3/4} k^{3/2}}{\kappa y_{IB}} \quad (11)$$

where $C_k = -0.416$ and $B_k = 8.366$. The implementation of k_{IB} and ε_{IB} are similar to the wall functions for k and ε used in OpenFOAM (OpenFOAM Foundation 2017).

5) Fix the values of flow variables on the IB cell centers when solving the momentum equation and the transport equations for k and ε.

6) Adjust the flux balance on the faces of IB cell centers on the solid side for mass conservation.

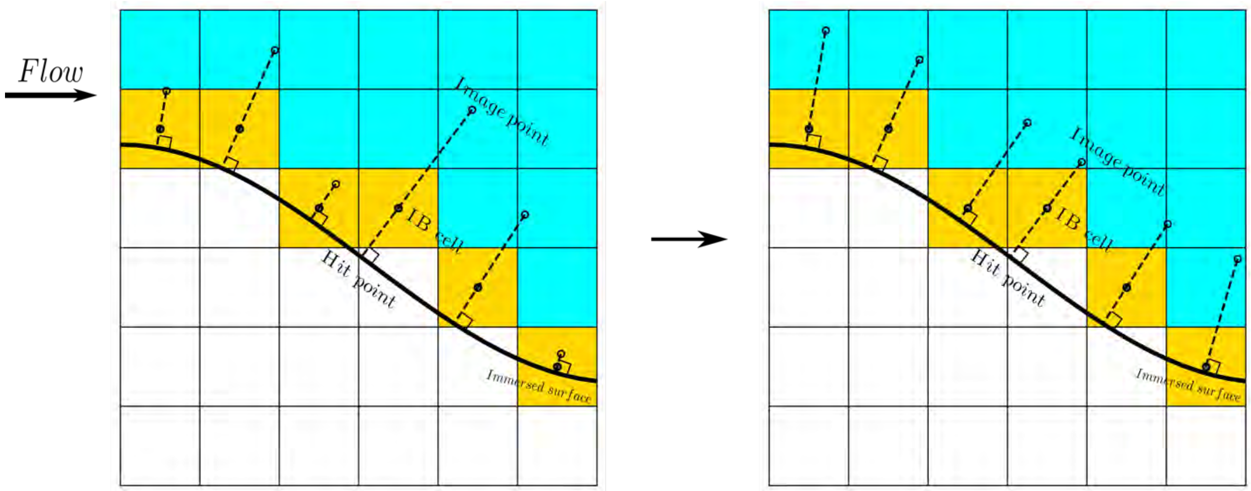

a) IB model: $y_{IP} = 3\, y_{IB}$ b) IB model: $y_{IP} = 3l_*$

Fig. 1: A schematic illustrating the IB models using a two-dimensional (2D) mesh.

The key to the IB treatment is the estimation of the shear velocity u_τ, i.e., the calculation of y_{IP}^+. Considering the nonlinear and discontinuous nature of velocity profile between the laminar sublayer and log-law sublayer, the result of y_{IP}^+ converges to different values if different velocity profiles are used. To keep the consistency when estimating the shear velocity u_τ of all IB cells, Eq. 7 assumes that the image points are located within the log-law sublayer such that only the log-law velocity profile is used in the iteration. Generally, the image point distance y_{IP} is proportional to the wall distance y_{IB} (for example, $y_{IP} = 3y_{IB}$) as shown in Fig. 1a (Balaras and Elias 2004; Seo et al. 2011). However, the wall distance y_{IB} is arbitrarily distributed around the immersed surface, making it impossible to guarantee that the image point is located in the logarithmic sublayer. In addition, an extremely small value of y_{IP} may result in numerical instability and even divergence of the model. In this work, y_{IP} is set to be proportional to the minimum dimension l_* of each IB cell ($y_{IP} = 3l_*$). Consequently, the image points are uniformly distributed along the immersed surface as shown in Fig. 1b. The numerical instability due to the small value of y_{IP} is avoided. A similar implementation has been used in Capizzano (2011) and Tamaki et al. (2017) for $k - \omega$ model and SA model.

Another problem in the near-wall treatment of the immersed boundary method comes from the inconsistency when the IB cell center and its corresponding image point are located in different sublayers of the velocity profile. Although all image points are designed to be in the log-law layer, the wall distance y_{IB} is still an arbitrary value and the IB cell center may be in the laminar sublayer. Therefore, Eq. 9, which assumes the IB cell center and image point follow the same logarithmic velocity profile, is not applicable in this situation. To address this problem, a modified velocity profile is used when the IB cell center is in the laminar sublayer. We assume a linear velocity profile between the wall and the image point such that the first derivative of the velocity with respect to the wall distance is still a constant ($\partial u/\partial y = \text{const.}$)(Fig. 2a). This method was proposed in Tamaki et al. (2017) to correct the mass flux on the cell boundary by using a slip velocity boundary condition. Here, it is used to extend the logarithmic velocity profile to the wall when the IB cell center is in the laminar sublayer. The eddy viscosity is also modified to be a constant between the wall and the image point (Fig. 2b). Thus, k_{IB}, and ε_{IB} are constant in this region. This modification is based on the balance of shear stress on the boundary:

$$(\upsilon + \upsilon_t)\left(\frac{\partial u}{\partial y}\right) = u_\tau^2 = \text{const.} \tag{12}$$

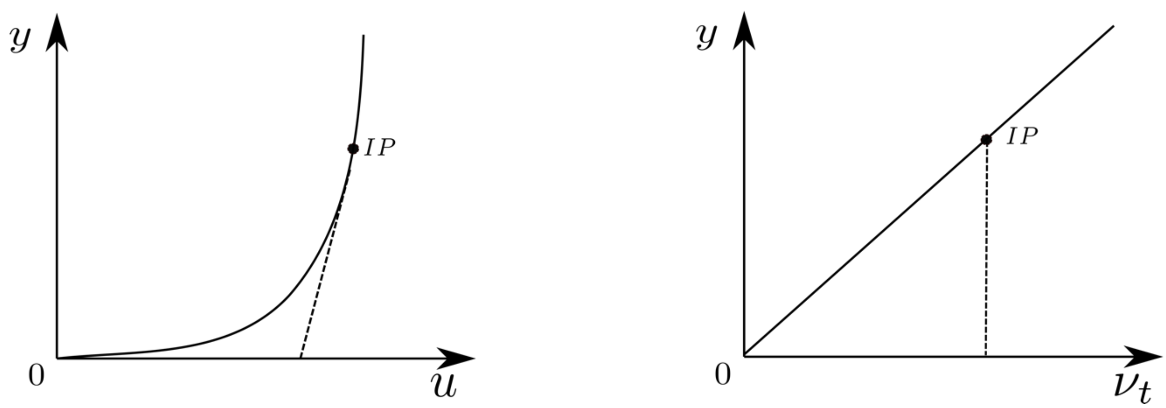

(a) Velocity profile (b) Eddy viscosity profile

Fig. 2: Velocity and eddy viscosity profile in the near-wall region. The solid lines are the original profiles. The dash lines are the modified profiles between the image point and the wall.

The modified flow velocity U_{IB}, k_{IB}, and ε_{IB} at the IB cell center are calculated as following:

$$U_{IB}^{new} = \begin{cases} U_{IP} - \frac{1}{\kappa} u_\tau \log\left(\frac{y_{IP}}{y_{IB}}\right) & \text{if } y_{IB}^+ > y_{Laminar}^+ \\ U_{IP} - \left(\frac{\partial u^+}{\partial y^+}\right)_{IP} (y_{IP} - y_{IB})\, u_\tau & \text{if } y_{IB}^+ \leq y_{Laminar}^+ \end{cases} \tag{13}$$

$$k_{IB} = \begin{cases} \frac{C_k \log(y_{IB}^+)}{\kappa} + B_k & \text{if } y_{IB}^+ > y_{Laminar}^+ \\ \frac{C_k \log(y_{IP}^+)}{\kappa} + B_k & \text{if } y_{IB}^+ \leq y_{Laminar}^+ \end{cases} \tag{14}$$

$$\varepsilon_{IB} = \begin{cases} \frac{C_\mu^{3/4} k^{3/2}}{\kappa y_{IB}} & \text{if } y_{IB}^+ > y_{Laminar}^+ \\ \frac{C_\mu^{3/4} k^{3/2}}{\kappa y_{IP}} & \text{if } y_{IB}^+ \leq y_{Laminar}^+ \end{cases} \tag{15}$$

where $\partial u^+/\partial y^+ = 1/(\kappa y^+)$. In the following, this is called the modified wall model and the one presented before is called the original model.

4. Results

The above IB method is implemented into U²RANS model. In this section, a number of turbulent flow cases are selected to verify the improved IB method. In particular, model accuracy is examined and discussed.

4.1 Turbulent flow over flat plate

The flow over a flat plate was used to investigate a 2D boundary layer without pressure gradient. The case is used to verify the IB method implementation with the proposed wall function. The length L of the plate is 2 m. The Reynolds number based on the plate length is $Re_L = 5 \times 10^6$ and incoming flow velocity is U = 2.5 m/s. The upper boundary is 0.1L away from the flat plate. The Cartesian mesh is refined near the leading edge and the plate. The mesh arrangement is shown in Fig. 3. A short slip surface (0.1L) is added in front of the leading edge using the symmetric boundary condition. The flat plate is modeled as an immersed boundary and the wall boundary condition is applied on it. We tested 4 different mesh size by using 4 different cell expansion ratios, $R_y = 1,5,10,20$, in the y-direction to change the mesh size of the first cell touching the wall. The cell expansion ratio, R, is that of the size of the end cell Δ_{x_N} to the size of the start cell Δ_{x_1} along the edge direction ($R = \Delta_{x_N}/\Delta_{x_1}$). Different mesh sizes change the value of y_{IB} and y_{IP}. For both original and modified wall models, the computed local friction coefficient (C_f) along the plate compares well with the experimental data from Weighart and Tillman (1951) (Fig. 4a and b); the velocity profiles at 0.9L are in good agreement with the log law (Fig. 4c and d). In addition, as y_{IB}^+ decreases, the simulation results converge to the experimental data. The results show that the proposed IB algorithm with original or modified wall model is insensitive to the image point distance y_{IP} in the log-law layer.

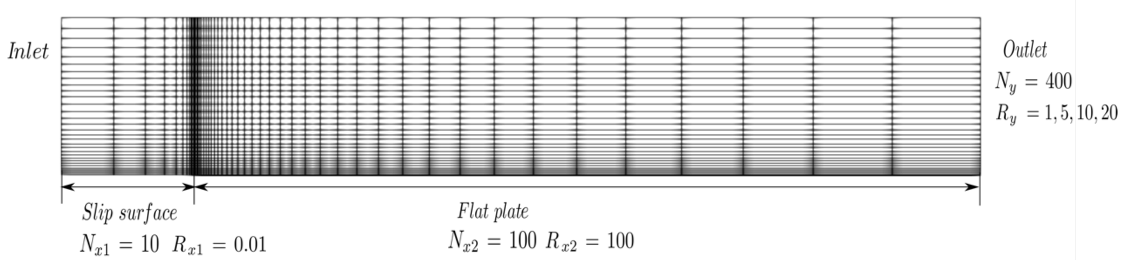

Fig. 3: Mesh for turbulence flow over a flat plate. *N* is the number of cells and *R* is the cell expansion ratio in each direction.

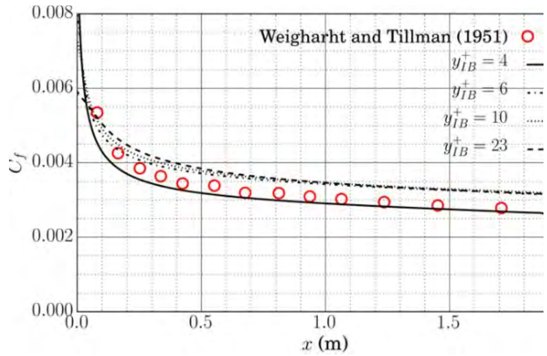

(a) Local friction coeffcient (original)

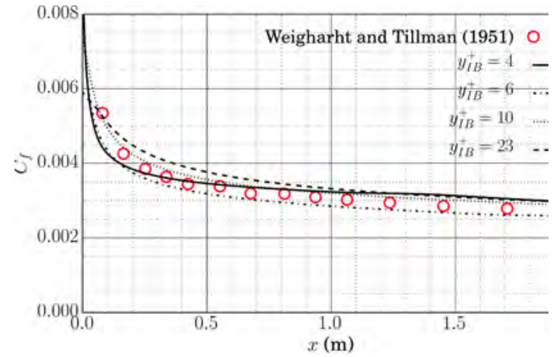

(b) Local friction coeffcient (modified)

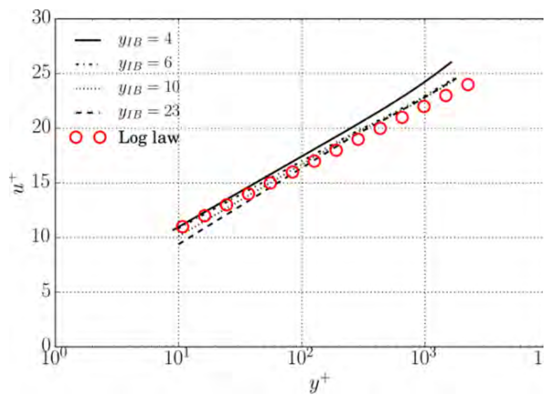

(c) Velocity profile at $0.9L$ (original)

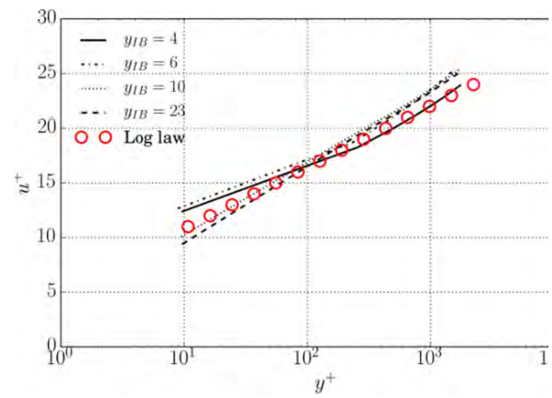

(d) Velocity profile at $0.9L$ (modified)

Fig. 4: Flat plate flow: simulated local friction coeffcient ($C_f = \tau_w / \frac{1}{2}\rho U^2$) and velocity profile at $0.9L$ of the plate using original and modified wall models. The aligned mesh is used.

To further investigate the stability of the algorithm and its dependence on wall distance, the mesh above the flat plate is rotated as shown in Fig.5. The top line of the grid has the same height to maintain the same water depth throughout the length. The bottom of the mesh is rotated and the downstream end of the bottom is moved down by $0.0025L$. The red line represents the position of the flat plate. With this configuation, the mesh lines are not aligned with the flat plate. As the grid rotates (stretches), the wall distance is not uniformly distributed along the plate. Other detail of the mesh arrangement is shown in Fig.5. N_{y2} is the number of mesh refinement in y-direction used in the region between the bottom line and the line $0.1L$ away from the bottom. We changed the number of N_{y2} ($N_{y2} = 100, 200, 300$) to show the mesh independence of this method. The cell expansion ratio in the y-direction in the refinemnt zone is 1 to maintain the minimum dimension l_* constant for each IB cell such that the image point distance is the same; but the wall distance distribution is nonuniform over the plate. Fig. 6a shows the numerical results of local friction coefficient using the original wall model. The predicted results are comparable with the experiment. However, there are some small, semi-periodic oscillations due to the change of wall distance along the plate, especially when the value of y_{IB} decreases and the IB cell center is in the laminar sublayer. To suppress the oscillation from the nonuniform wall distance, the modified wall model is applied and the simulated results are plotted in Fig. 6b. The modified wall model can predict the local friction coefficient more accurately and the oscillation is greatly reduced. As the mesh is refined, the local friction coefficient converges to the experimental data. In addition, velocity profiles in Fig. 6b and d at $0.9L$ agree well with the log-law. Both the original and modified wall models give a good prediction of velocity.

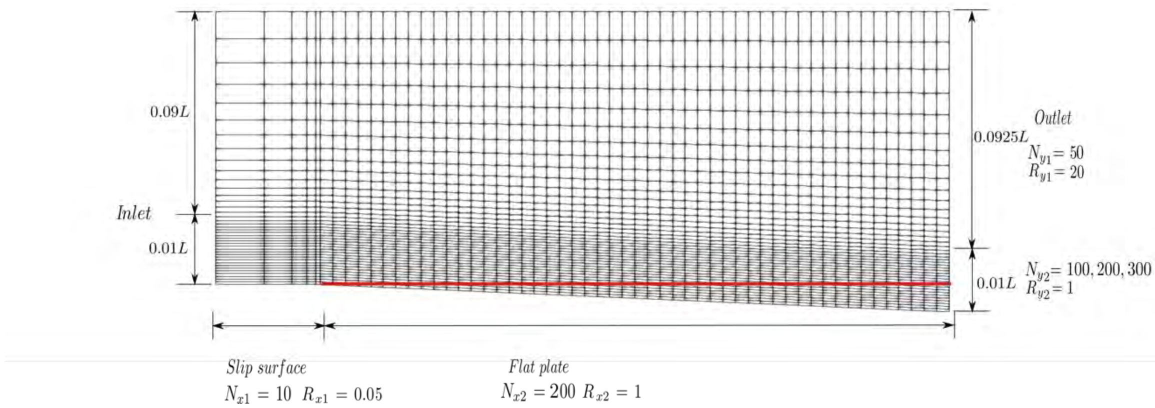

Fig. 5: Sketch of the rotated (stretched) mesh for turbulence flow over a flat plate.

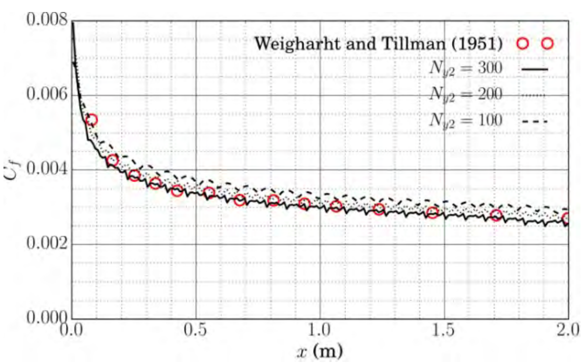

(a) Local friction coeffcient (original)

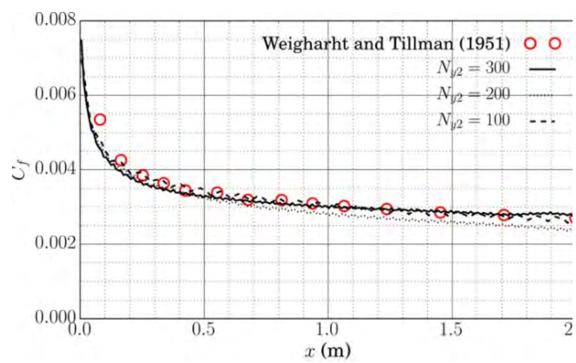

(b) Local friction coeffcient (modified)

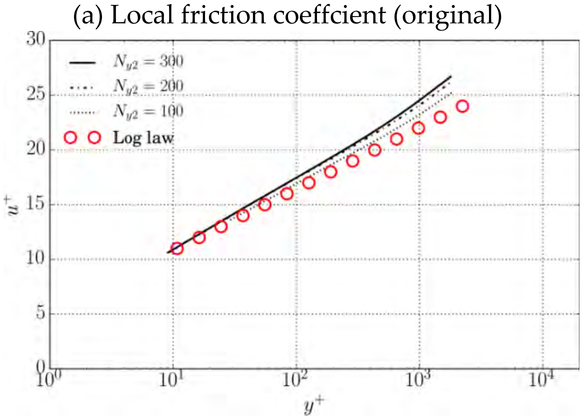

(c) Velocity profile at $0.9L$ (original)

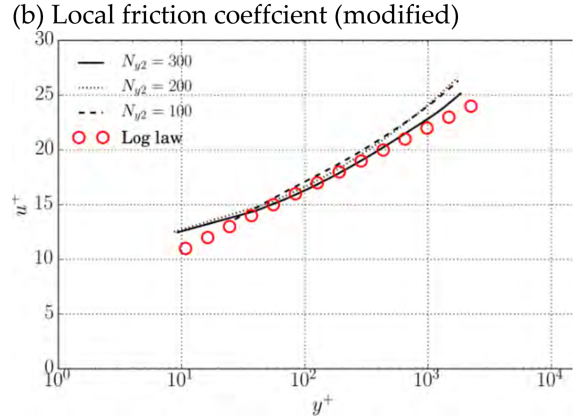

(d) Velocity profile at $0.9L$ (modified)

Fig. 6: Flat plate flow: simulated local friction coefficient ($C_f = \tau_w / \frac{1}{2}\rho U^2$) and velocity profile at $0.9L$ of the plate using original and modified wall models. The rotated mesh is used.

4.2 Turbulent flow around a cylinder over scoured beds

The proposed IB algorithm is verified next for its capability to simulate a case with an instream structure - a turbulent flow around an instream cylinder over scoured beds. The modified wall model is used. The simulated results are compared with the flume experiment by Jensen et al. (1990). Fig. 7 shows the three bed profiles representing three scour phases observed in the experiment by Mao (1986). The cylinder has a diameter of 3 cm and is placed above three scoured bed profiles. The mean inlet flow velocity is 0.2 m/s. The computational domain is 1.1 m in the streamwise direction (*x*-direction). The flow depth at uneroded bed at the exit is maintained at 0.245 m (*y*-direction). Despite 2D flow in nature, the modeling is carried out in a 3D model domain with the dimension of 0.03 m along the cylinder (*z*-direction).

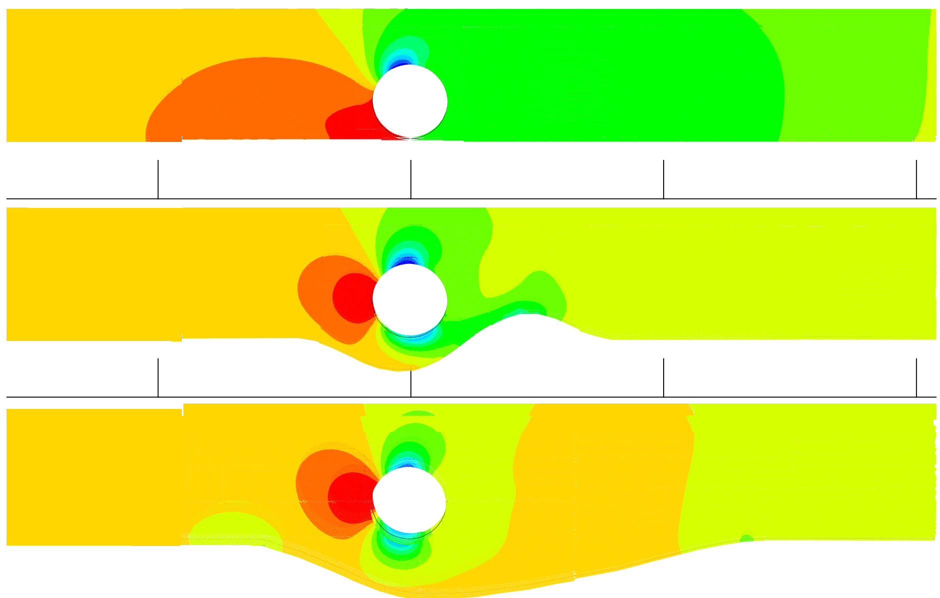

Fig. 7: Three cases are simulated corresponding to three bed profiles; the top, middle and bottom profiles correspond to profile 1, 3 and 5, respectively, of the experiments in Jensen et al. (1990). The simulated pressure contours are also displayed.

Using profile 3 as an example, the Cartesian background mesh has 0.1 cm resolution near the cylinder and scour bed, which is the finest resolution similarly used by Smith and Foster (2005). The background mesh has a total of 355,515 3D cells (71,103 2D cells in the xy plane and 5 cells along z). The cylinder boundary and bed profiles are treated as the immersed boundaries. The fluid and IB cells near the immersed boundaries are shown in Fig. 8. The meshes for the two other profiles are similar.

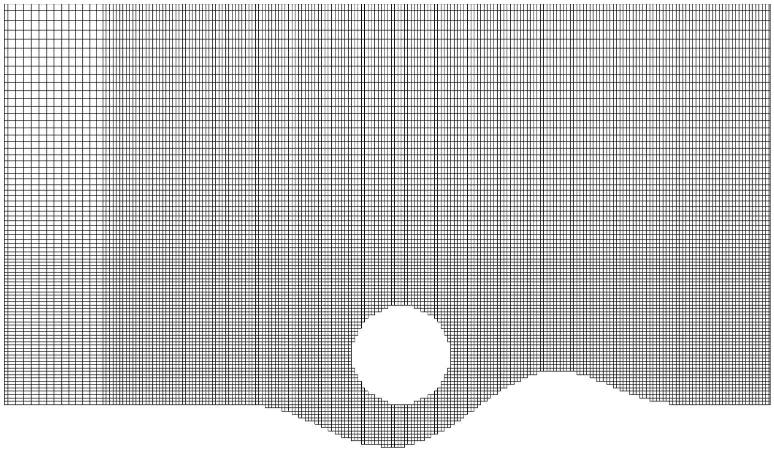

Fig. 8: Close-up side views of the fluid mesh cells near the cylinder and bed profile 3.

Fig. 9 shows the comparisons between simulation results and measured data from experiments. It is seen that the computed vertical (y) velocity profile approaching the cylinder is near-logarithmic although a constant velocity boundary condition is applied at the inlet. The IB method simulated velocity profiles agree well with the experimental data for all three profiles and at eight streamwise stations. The results show that the recovery from the cylinder is slow - even at the last measured location about eight cylinder diameters downstream (x=24 cm) the wake effect of the cylinder is still significant.

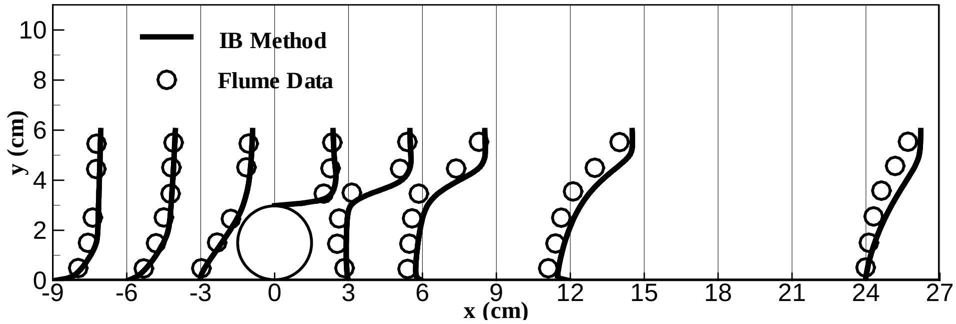

(d) Profile 1

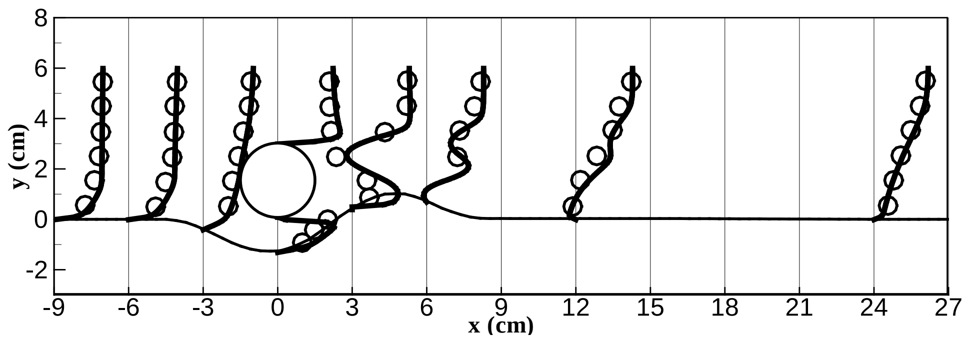

(e) Profile 3

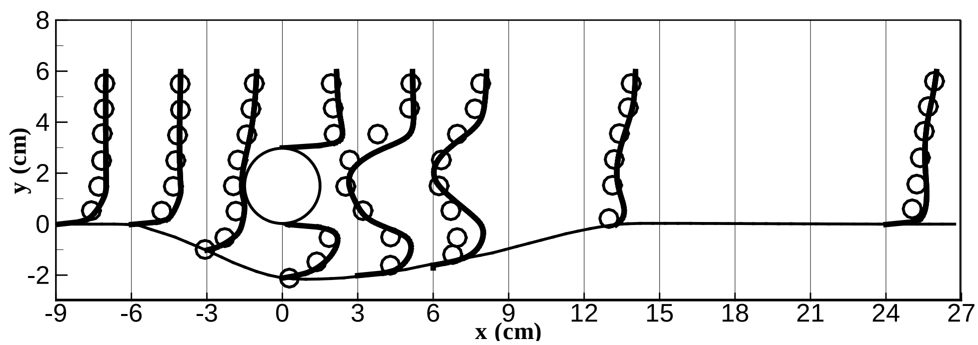

(f) Profile 5

Fig. 9: Comparisons of the predicted streamwise velocity (U) with the measured data along eight streamwise stations. Scaling of U is such that one unit of x is 10 cm/s.

4.3 Turbulent flow over 3D dunes

3D dunes were used to verify the model performance with the turbulence model in a 3D form, especially, the prediction of wall shear stress. The modified wall model is used in this case for a more accurate and smooth wall shear prediction. The simulation results are compared with the experiments of Maddux et al (2003a). In the experiment, fourteen fixed 3D dunes were placed on the bottom of the flume sequentially and experimental data were measured on the eleventh and twelfth numbered dunes. Only 6 dunes are simulated to reduce the computational cost and the data were collected from the last two dunes as shown in Fig. 10a. The length of the simulation domain is 5.0 m in the x-direction and the width of the domain is 0.9 m in the y-direction. The bed elevation contour of the 3D dunes is shown in Fig. 10b. The incoming velocity is 0.261 m/s in the x-direction and the water depth is 0.561 m in z-direction.

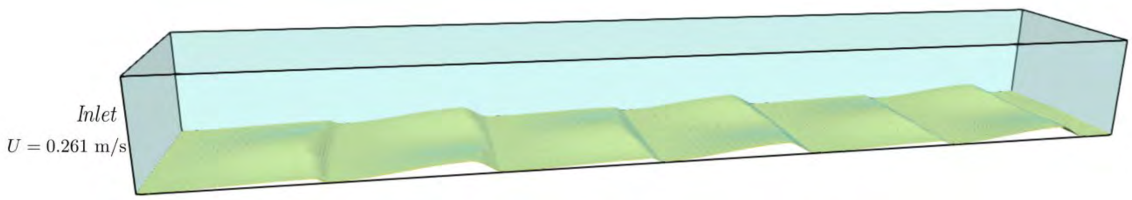

(a) Sketch of the computational domain

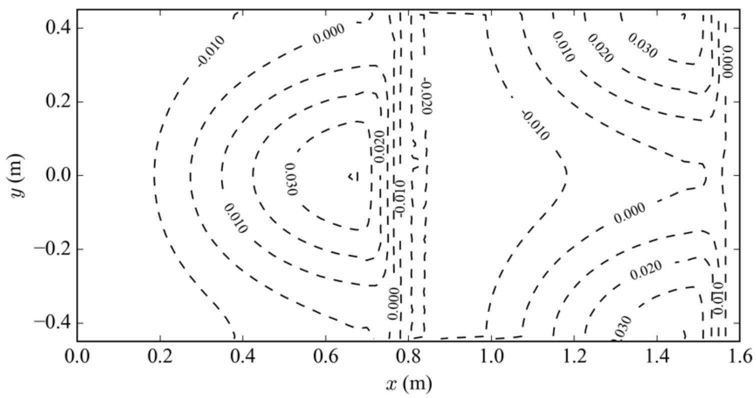

(b) Bed elevation of the 3D dunes in meters

Fig. 10: Simulation domain and bed boundary.

The Cartesian background mesh is shown in Fig. 11. The numbers of cells are 450, 90, and 70 in the x, y and z direction, respectively. The mesh is refined near the dunes, especially where the bed elevation changes rapidly.

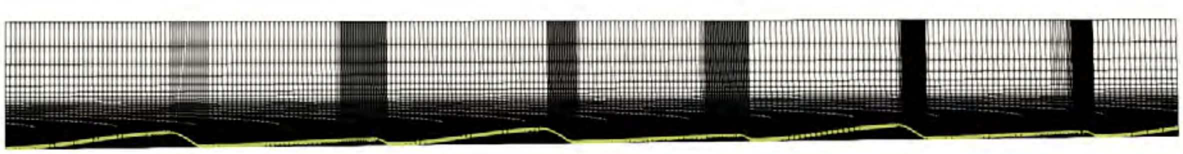

Fig. 11: Mesh for flow over 3D dunes.

Fig. 12 is a comparison of results from the IB method and the experiment. The streamwise velocities at different locations are well predicted. The only noticeable deviation is at the downstream of the measured two dunes at $y = 0$ m. In this slice, the bed elevation has the largest slope such that a long distance from the inlet is required for the flow to be fully developed. In the experiment, the measured dunes are the eleventh and twelfth. However, the measured dunes in the simulation are at the fifth and sixth due to the limitation of computing capacity. Thus, the flow condition is slightly different.

Comparison of bed shear stress is shown in Fig. 13. The simulation results show that the new IB algorithm can provide a smooth wall shear stress distribution. The normalized wall shear stress of the measured data (Fig. 13a) is estimated using the velocity 5 mm above the bed (Maddux et al., 2003b).:

$$|\tau_b| = u_\tau^2 = \left|\frac{30\kappa U_1}{\ln(z_1 - \eta)/k_s}\right|^2 \tag{12}$$

where U_1 is the velocity at 5 mm above the bed, the distance $z_1 - \eta$ is 5 mm, and $k_s = 1$ mm is the bed roughness.

The wall shear stress u_τ^2 from the IB simulation is based on Eq. 7 and 8 and shown in Fig. 13b. Even with the distribution of IB cells and image points changing arbitrarily with the bed elevation, the predicted shear stress is smooth. A comparison with the experimental data in Fig. 13a shows the existence of mismatch between the two. This is mainly because the accuracy of the simulation is limited by the computing capacity such that the velocity prediction at the places with large slope deviates from the experiment. However, the general characteristics of the wall shear stress are captured by the numerical model. The wall shear stress is the highest at the crests of dunes and relatively small elsewhere. The smooth distribution of wall shear stress is very important for modeling the sediment transport and scours, which is currently under development.

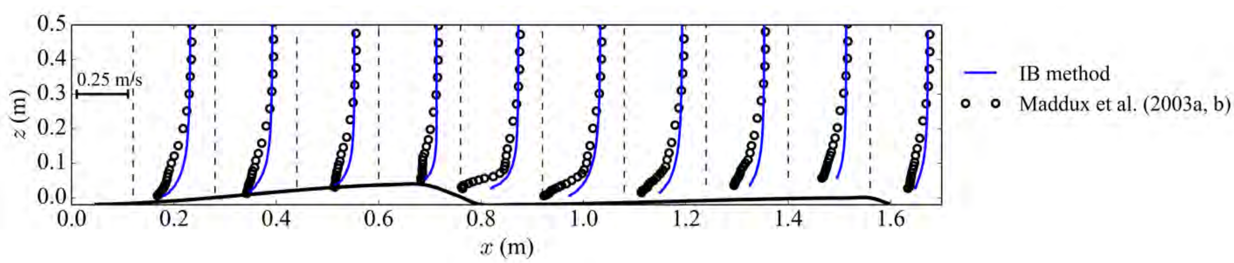

(a) The streamwise velocity at $y = 0$ m

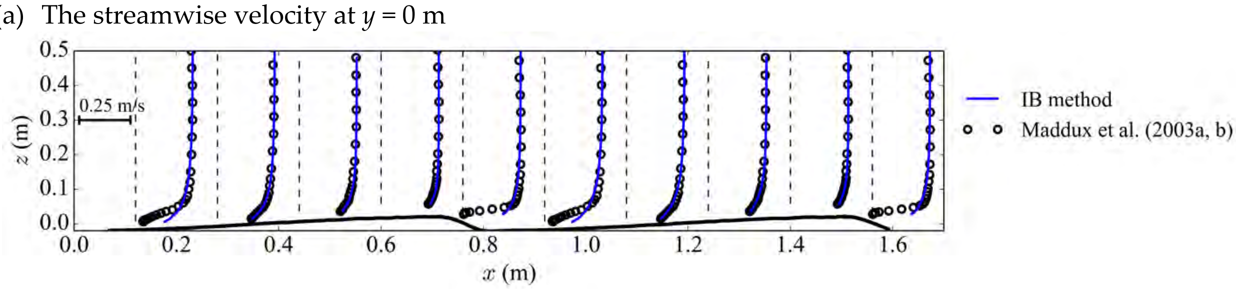

(b) The streamwise velocity at $y = 0.225$ m

Fig. 12: The comparison of streamwise velocity from simulation and experiment.

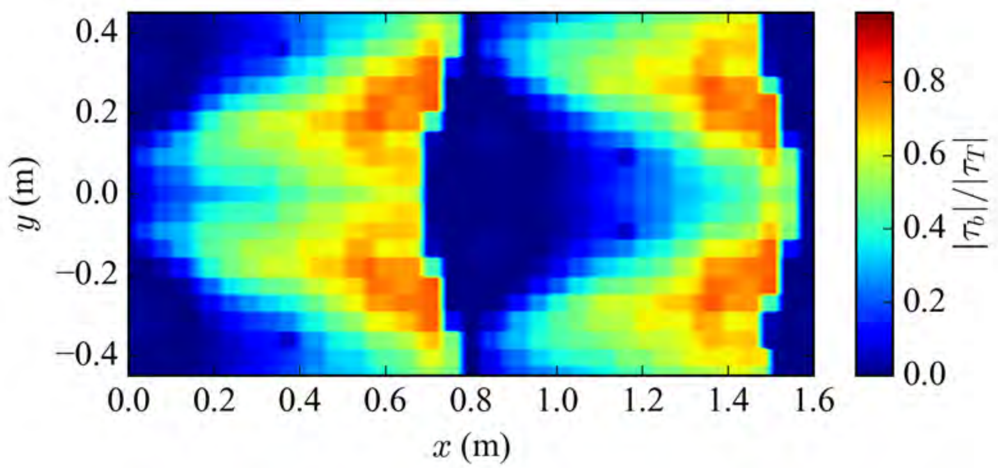

(a) Normalized wall shear stress from Maddux et al (2003b), $|\tau_T|$ = 0.00046 m²/s.

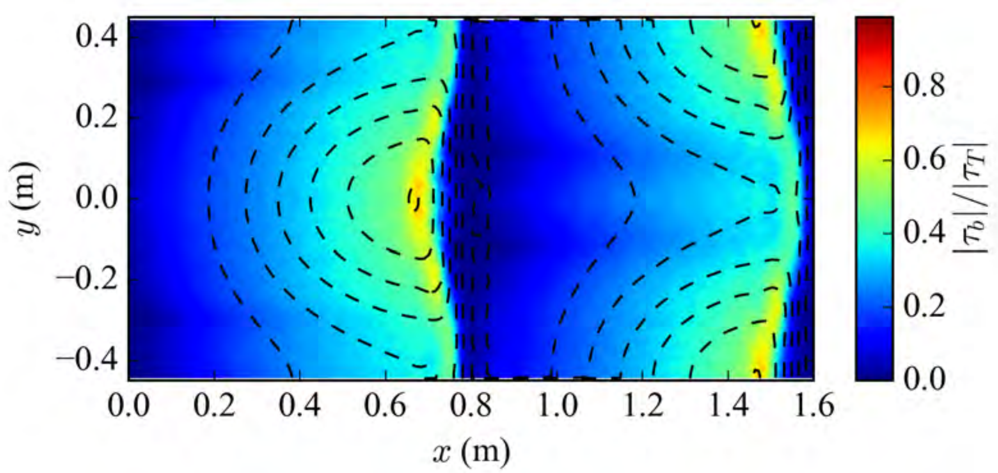

(b) Normalized wall shear stress from IB method

Fig. 13: Normalized wall shear stress contours from simulation and experiment.

5. Conclusion

This work proposes a new wall model algorithm for use by the IB method in association with the $k-\varepsilon$ turbulence model. It is implemented into the terrain-conforming U²RANS model of Lai et al. (2003). The aim is to develop a flexible IB-method based CFD model so that turbulent flow filed can be simulated accurately and smooth wall shear stress can be generated. A key contribution is to use a consistent velocity profile – log-law velocity profile – to estimate the wall shear velocity. In addition, a modification is proposed in the wall model for the laminar sublayer to suppress the oscillation caused by the small value of wall distance y_{IB}. In such a way, the discontinuity and nonlinearity of the velocity profile between the laminar sublayer and log-law sublayer are avoided. The new method was tested and validated with selected 1D, 2D, and 3D flow cases. Good results are obtained in each case. The proposed method produces an accurate and smooth wall shear stress distribution, paving the way for the next stage of model development for sediment transport and scour modeling.

References

1. Mittal, R. and G. Iaccarino, Immersed boundary methods. Annu. Rev. Fluid Mech., 2005. 37: p. 239-261.
2. Mohd-Yusof, J., For simulations of flow in complex geometries. Annual Research Briefs, 1997. 317: p. 35.
3. Verzicco, R., et al. LES in complex geometries using boundary body forces. in Proceedings of the summer program. 1998.
4. Coclite, A., et al., *Kinematic and dynamic forcing strategies for predicting the transport of inertial capsules via a combined lattice Boltzmann–immersed boundary method.* Computers & Fluids, 2019. **180**: p. 41-53.
5. Kim, J., D. Kim, and H. Choi, An immersed-boundary finite-volume method for simulations of flow in complex geometries. Journal of computational physics, 2001. 171(1): p. 132-150.
6. Tessicini, F., et al., Wall modeling for large-eddy simulation using an immersed boundary method. Annual Research Briefs, 2002: p. 181-187.
7. Harada, M., et al. A Novel Simple Cut-Cell Method for Robust Flow Simulation on Cartesian Grids. in 54th AIAA Aerospace Sciences Meeting. 2016.
8. Roman, F., et al., An improved immersed boundary method for curvilinear grids. Computers & fluids, 2009. 38(8): p. 1510-1527.
9. Yang, X., et al., Integral wall model for large eddy simulations of wall-bounded turbulent flows. Physics of Fluids, 2015. 27(2): p. 025112.
10. Termini, D., Bed scouring downstream of hydraulic structures under steady flow conditions: Experimental analysis of space and time scales and implications for mathematical modeling. Catena, 2011. 84(3): p. 125-135.
11. Tamaki, Y., M. Harada, and T. Imamura, Near-wall modification of Spalart–Allmaras turbulence model for immersed boundary method. AIAA Journal, 2017. 55(9): p. 3027-3039.
12. Capizzano, F., Turbulent wall model for immersed boundary methods. AIAA journal, 2011. 49(11): p. 2367-2381.
13. Zhou, C., RANS simulation of high-Re turbulent flows using an immersed boundary method in conjunction with wall modeling. Computers & Fluids, 2017. 143: p. 73-89.
14. Lai, Y.G., L.J. Weber, and V. Patel, Nonhydrostatic three-dimensional method for hydraulic flow simulation. I: Formulation and verification. Journal of Hydraulic Engineering, 2003. 129(3): p. 196–205.

15. Lai, Y.G., 3D CFD Simulation: Terrain-Conforming versus Terrain-Embedding Method. ASCE World Environmental and Water Resources Congress, Henderson, NV, May 17-21. 2020.
16. Song, Y., Lai, Y.G., and Liu, X., Improved adaptive immersed boundary method for smooth wall shear. ASCE World Environmental and Water Resources Congress, Henderson, NV, May 17-21. 2020.
17. Launder, B.E. and D.B. Spalding, The numerical computation of turbulent flows, in Numerical prediction of flow, heat transfer, turbulence and combustion. 1983, Elsevier. p. 96-116.
18. Greenshields, C.J., The OpenFOAM Foundation." User Guide version 6". 2018, OpenFOAM Foundation Ltd.
19. Balaras, E., Modeling complex boundaries using an external force field on fixed Cartesian grids in large-eddy simulations. Computers & Fluids, 2004. 33(3): p. 375-404.
20. Seo, J.H. and R. Mittal, A high-order immersed boundary method for acoustic wave scattering and low-Mach number flow-induced sound in complex geometries. Journal of computational physics, 2011. 230(4): p. 1000-1019.
21. Wieghardt, K. and W. Tillmann, On the turbulent friction layer for rising pressure. 1951.
22. Jensen, B., et al., Flow around and forces on a pipeline near a scoured bed in steady current. 1990.
23. Mao, Y., The interaction between a pipeline and an erodible bed (PhD Thesis). Lyngby, Denmark: Technical University of Denmark, 1986.
24. Smith, H.D. and D.L. Foster, Modeling of flow around a cylinder over a scoured bed. Journal of waterway, port, coastal, and ocean engineering, 2005. 131(1): p. 14-24.
25. Maddux, T., J. Nelson, and S. McLean, Turbulent flow over three-dimensional dunes: 1. Free surface and flow response. Journal of Geophysical Research: Earth Surface, 2003. 108(F1).
26. Maddux, T., S. McLean, and J. Nelson, Turbulent flow over three-dimensional dunes: 2. Fluid and bed stresses. Journal of Geophysical Research: Earth Surface, 2003. 108(F1).

Appendix B. Comparative Study Paper

3D CFD Simulation: Terrain-Conforming versus Terrain-Embedding Method

Yong G. Lai, Ph.D.[1]

[1]Technical Service Center, U.S. Bureau of Reclamation, P.O. Box 25007, Denver, CO 80225; e-mail: ylai@usbr.gov

ABSTRACT

Three-dimensional (3D) computational fluid dynamic (CFD) simulation is gaining popularity in recent years for stream flow modelling. It is necessary when local flow patterns are of interest and/or there exist in-stream structures. Representation of complex terrain, however, is a major obstacle in 3D CFD modelling. Traditionally, the terrain-conforming method is widely used in which terrains are accurately represented by a 3D mesh; i.e., the mesh conforms to the terrain geometry. This method is straightforward in implementation and accurate in resolving the near-terrain flows. A drawback is that such a mesh is difficult to generate when the terrains are complex. The mesh quality may become too poor to maintain solution stability and accuracy. An alternative is the terrain-embedding method with which terrains are embedded in a background mesh. The background mesh may be generated without the requirement of conforming to the terrain so that mesh generation is relatively simple and good mesh quality may be maintained. Special algorithm, however, is needed to take into account the effect of the embedded terrains on the nearby flow. In this study, both CFD methods are adopted to simulate a selected flow case. The objective is to understand the pros and cons of the two methods through a real laboratory case, not merely in theory. The study is to pave a way to simulate sediment transport and scour cases when stream bed is moving.

INTRODUCTION

Non-hydrostatic 3D CFD models are the most general and accurate in simulating fluid flows. They are accurate as they adopt the least amount of empiricism in the mathematical formulation of fluid flows. More restrictive in modeling capability and less accurate in results are the currently popular models such as the cross-sectionally averaged 1D and depth-averaged 2D models. Currently, there are a number of 3D CFD models available commercially or in the public-domain; they are gaining popularity in hydraulic engineering applications. A surge in the use of 3D CFD models is due to the recent advances in numerical algorithm development, availability of public-domain models, and speedup of the computer software and hardware. A few reviews have been conducted specific to the hydraulic engineering, such as the reviews by Papanicolaou et al. (2008), ASCE Sedimentation Manual (2007), Liu and Zhang (2019).

3D CFD modelling is labor-intensive and demands high computing resources. There is a lack of user-friendly CFD models available to public use. A primary obstacle is that a good-quality 3D mesh is needed but difficult to generate, especially for streams with complex terrains. Most existing models adopt the terrain-conforming method in which terrains are accurately represented by the 3D mesh; i.e., the mesh conforms to the terrain geometry. This method is straightforward in implementation and terrain boundary conditions may be accurately represented to resolve the near-terrain flows. A terrain-conforming mesh, however, is difficult to generate and the mesh quality is even harder to control. Poor mesh qualities may lead to solution instability and result inaccuracy.

In this study, we report a research effort seeking to develop a 3D model for practical usage in the hydraulic engineering. A key departure from the traditional models is the adoption of the terrain-embedding method. With such a method, a complex terrain is embedded in a background mesh which may be generated without the requirement of conforming to the terrain geometry. As a result, mesh generation is relatively simple and mesh quality may be maintained good. Special algorithm, of course, is needed to take into account the effect of the embedded terrains on the near-terrain flow. There are various types of the terrain-embedding method. In this study, a special immersed boundary method is adopted, which was developed into OpenFOAM (Open source Field Operation and Manipulation) as reported by Xu and Liu (2019). Herein, the algorithm is implemented into the CFD model of Lai et al. (2003) named U^2RANS. The theory part of the new terrain-embedding capability of U^2RANS is reported in a companioning paper by Song et al. (2020). This paper focuses on the comparison of both the terrain-conforming and terrain-embedding methods with a laboratory flume case. The objective is to understand the pros and cons of the two methods through a real case, not merely in theory. The study is to pave a way to simulate sediment transport and scour cases when stream bed is moving in the next phase. The terrain-embedding method is expected to hold a big advantage over the terrain-conforming method for moving-boundary problems such as scour processes. The ultimate goal is to develop a 3D CFD model that is robust, reliable, user-friendly, and free-availability to the public.

LITERATURE REVIEW

A brief review is provided below with regard to the development of CFD models. The discussion focuses on non-commercial models only and is limited to the ones based on the Reynolds-Averaged Navier-Stokes (RANS) equations.

Early 3D RANS models were developed by Demuren (1993), Olsen and Melaaen (1993), Behr and Tezduyar (1994), Casulli (1997), Berger and Stockstill (1999), among many others. The models belonged mostly to the terrain-conforming type and adopted finite-difference or finite-volume models with the structured grids (hex cells) and finite-element models with the unstructured grids (purely hex or tetrahedrons).

Mahadevan et al. (1996a, b) reported a weakly non-hydrostatic ocean model which adopted a boundary-fitted curvilinear sigma mesh. A similar model was developed by Casulli and Stelling (1998) but orthogonal mesh was required in the horizontal plane and Z-grid was adopted in the vertical direction. A truly non-hydrostatic CFD model, named TRIM_3D, was proposed by Casulli (1999). The above models adopted the fractional step method. Later, Lai et al. (2003) developed a finite-volume unstructured mesh model using the pressure-correction method; the model was named U^2RANS. A key feature of U^2RANS was that the mesh may assume flexible shapes (polyhedrons) and is the most general in its category. Fringer et al. (2006) also developed a model based on the pressure correction method; it was named SUNTANS for coastal and ocean simulations. The pressure-correction method was evaluated by Armfield and Street (2002) to have a higher order of convergence with respect to the time step than the fractional step method. A similar pressure-correction method was adopted by Ullmann (2008) with the Z-mesh formulation.

Most CFD models were developed for research purpose and not general for public use. One exception is the public-domain model OpenFOAM, which is a toolbox for the development of customized numerical solvers including forming a CFD model. The advantages of OpenFOAM include, but not limited to: (a) friendly syntax for partial differential equations; (b) unstructured polyhedral grid capabilities; (c) automatic model parallelization; (d) wide range of applications. The model, however, is not easy to use and suited primarily for CFD experts. Model customization is challenging with increasing depth into the OpenFOAM library. The learning curve is steep due to the absence of an integrated graphical user interface and insufficient technical and usage documentation.

Another model available to the public is based on the works of Olsen and Melaaen (1993), Olsen (1994), and Olsen and Kjellesvig (1998). The model is named SSIIM which adopts the unstructured finite volume method. A unique feature of SSIIM is that it solves both the hydrodynamic and sediment transport equations with a movable riverbed. Other models are less popular in usage and a few are mentioned. Bihs et al. (2013) developed an open-source CFD model named REEF3D. The level-set method was used to calculate the moveable surfaces. A 3D model was reported by Jia (2013), named CCHE3Dm which was based on the finite element and collocation method. CCHE3D has been demonstrated with a number of practical project applications with sediment transport capabilities. A comprehensive 3D model, VSL3D, was developed by Professor Sotiropoulos and his colleagues. A detailed description of the model may be found in Khosronejad et al. (2014). VSL3D is a 3D flow and mobile-bed model capable of simulating turbulent flow and sediment transport in natural waterways with arbitrarily complex hydraulic structures. Geometric complexity is handled using the curvilinear immersed boundary (CURVIB) approach of Ge and Sotiropoulos (2007) and the wall modeling approach of Kang et al. (2011).

MATHEMATICAL EQUATIONS

The 3D CFD model of U^2RANS is based on unstructured, arbitrarily shaped mesh cell model of Lai et al. (2003). U^2RANS solves the standard Reynolds averaged Navier-Stokes (RANS) equations as follows:

$$\frac{\partial U_j}{\partial x_j} = 0$$

$$\frac{\partial U_i}{\partial t} + \frac{\partial U_i U_j}{\partial x_j} = \frac{\partial}{\partial x_j}\left(\upsilon \frac{\partial U_i}{\partial x_j} + \tau_{ij} \right) - \frac{\partial P / \rho}{\partial x_i} + g_i$$

In the above, t is time; x_j is the j-th Cartesian coordinate; ρ is the water-sediment mixture density; U_j is the mean velocity components along the Cartesian coordinate x_j; $\tau_{ij} = -\overline{u_i u_j}$ is the turbulence stress with u_j the j-th turbulent fluctuating velocity component; P is the mean pressure; υ is the mixture viscosity; and g_i is the i-th component of the acceleration due to gravity.

A turbulence model is used to relate the Reynolds stress tensor τ_{ij} to other variables. The standard k-ε model of Launder and Spalding (1974) is adopted as:

$$\tau_{ij} = \upsilon_t \left(\frac{\partial U_i}{\partial x_j} + \frac{\partial U_j}{\partial x_i} \right) - \frac{2}{3} k \delta_{ij}$$

where δ_{ij} is the Kronecker delta (a unit tensor) and the eddy viscosity is obtained from:

$$\upsilon_t = C_\mu \frac{k^2}{\varepsilon}$$

In the above, k is the turbulence kinetic energy and ε is the turbulence dissipation rate.

The transport equations for k and ε may be expressed as:

$$\frac{\partial k}{\partial t} + \frac{\partial U_j k}{\partial x_j} = \frac{\partial}{\partial x_j}\left((\upsilon + \frac{\upsilon_t}{\sigma_k}) \frac{\partial k}{\partial x_j} \right) + G - \varepsilon$$

$$\frac{\partial \varepsilon}{\partial t} + \frac{\partial U_j \varepsilon}{\partial x_j} = \frac{\partial}{\partial x_j}\left((\upsilon + \frac{\upsilon_t}{\sigma_\varepsilon}) \frac{\partial \varepsilon}{\partial x_j} \right) + C_{\varepsilon 1} \frac{\varepsilon}{k} G - C_{\varepsilon 2} \frac{\varepsilon^2}{k}$$

where $G = \tau_{ij} \frac{\partial U_i}{\partial x_j}$ is the turbulence generation rate. The standard model constants take the following values:

$$C_\mu = 0.09;\ C_{\varepsilon 1} = 1.44,\ C_{\varepsilon 2} = 1.92,\ \sigma_k = 1.0,\ \sigma_\varepsilon = 1.3$$

The terrain-embedding method has been described y Song et al. (2020) and it is not repeated herein.

MESH PREPARATION

3D hydraulic modeling starts with the generation of a 3D mesh to represent the bathymetry of the river. In the past, the terrain-conforming method is widely used; the generation of a good-quality 3D mesh, however, has long been a grand challenge. In this study, the mesh generation of the terrain-conforming modeling of U^2RANS is achieved as follows. First, a background mesh is generated without regard to the terrains and inserted objects if they exist. Second, the terrain-conforming mesh is generated using the snappyHexMesh tool offered by OpenFOAM.

The 3D background mesh is generated in a two-step process. First, a 2D horizontal mesh is generated for which any 2D mesh generation packages may be used. The 2D mesh generation needs only to consider horizontal features such as stream boundaries and is relatively straightforward. Second, the 3D background mesh is generated by extruding the 2D mesh from the given water free surface towards the bed with a constant water depth. The free surface elevation may either be flat which is generally valid for a short-reach stream, or from a 2D simulation. The background mesh such generated is of the type of sigma mesh except that the bottom mesh does not conform to the stream bed. As a result, a good-quality mesh may be maintained. Other background mesh types may also be generated as described by Lai (2019); but the above is sufficient for most problems.

The final terrain-conforming mesh is generated using snappyHexMesh by the inputs of the background mesh, the stream bed terrain and any inserted objects. The “castellatedMesh” and “snap” modules are used to generate the terrain-conforming mesh. We found the “addLayers” module did not work well for most stream simulation cases, due probably to the high aspect ratio issue typical for hydraulic modeling.

With the terrain-embedding method, only the background mesh is needed. The above process of background mesh generation is followed.

MODEL VERIFICATION AND COMPARISON

Description of the Simulated Case

A flume case is selected to compare the terrain-conforming and terrain-embedding methods. It is a turbulent flow around a cylinder over scoured beds and the flume experiment was carried out by Jensen et al. (1990). In the test, the flume had the size of 10m X 0.3m X 0.3m. A cylinder of 3 cm diameter was placed above five scoured bed profiles and in a flowing water. The flow velocity was maintained at a constant speed of 0.2 m/s. The bed profiles represented different scour phases as observed by Mao (1986). Velocity and turbulence components were measured at various longitudinal (flow-wise) stations and the measured data may be used for comparisons with the CFD results. The same case was simulated using other CFD models in the past such as the study of Smith and Foster (2005) who used the commercial CFD model FLOW-3D.

In the present study, three bed profiles, shown in Figure 1, are selected for simulation with U^{2}RANS, corresponding to profile 1, 3 and 5. The CFD model domain is 1.1 m longitudinally along the flow direction (x), varying size vertically along the water depth direction (y), and 0.03 m laterally along the cylinder (z). At the inlet, the flow has a uniform velocity of 0.2 m/s so that the Reynolds number of the flow is 6,000 based on the approaching velocity and the cylinder diameter.

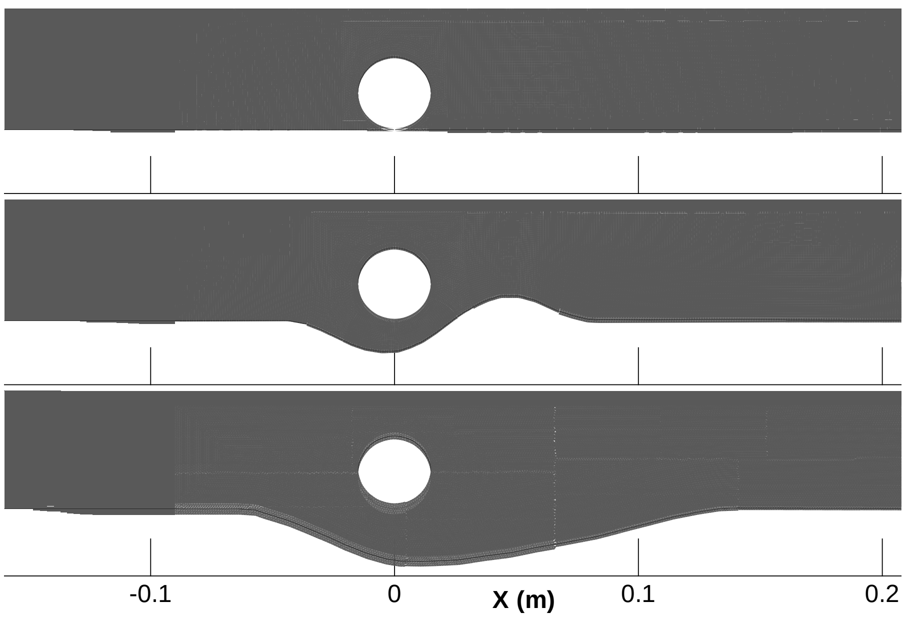

Figure 12. Three bed profiles simulated: top, middle and bottom profiles correspond to profile 1, 3 and 5, respectively, of the experiment of Jensen et al. (1990).

Numerical Model Inputs

The terrain-conforming model mesh conforms to both the cylinder and bed so that the water depth varies (approaching flow depth is 0.245 m). A closed-up view of the mesh for profile 3 is shown in Figure 2 as an example. A 2D mesh is generated first which is a combined quadrilateral and triangle cells in the x-y plane; the 3D mesh is then created by extruding the 2D mesh along the z direction. The 2D mesh has a total of 60,784 mesh cells. A much denser mesh resolution is used near the cylinder: mesh size is about 0.06 to 0.12 cm near the cylinder. With 5 cells used laterally, the 3D mesh has a total of 303,920 cells. Note that the mesh resolution is slightly finer than the finest resolution adopted by Smith and Foster (2005) to ensure that the results are almost mesh insensitive according to that study. Three meshes are generated corresponding to bed profile 1, 3 and 5, respectively, though only profile 3 mesh is discussed.

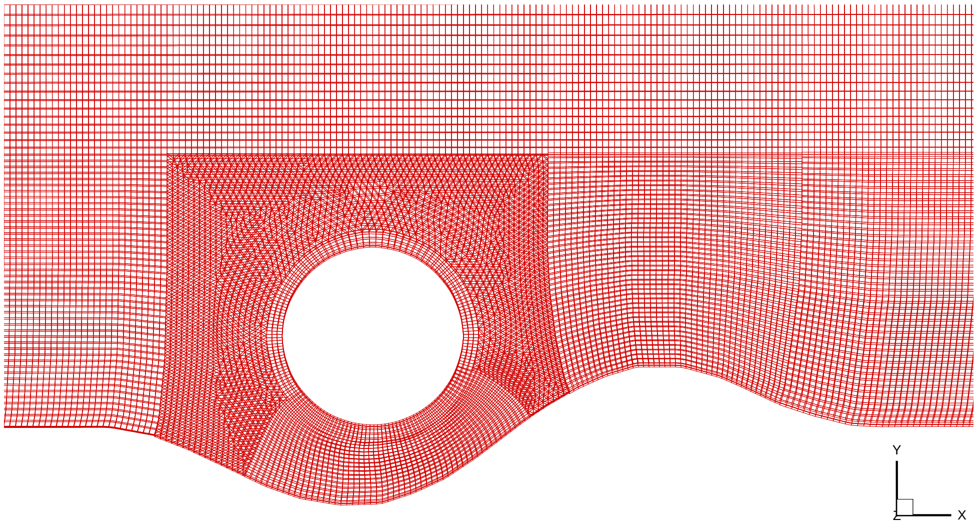

Figure 13. Terrain-conforming mesh for bed profile 3: a close-up view.

The terrain-embedding simulation needs only a background mesh which consists of rectangular mesh cells only; the model domain size is 1.1 m (x), by 0.27 m (y), by 0.03 m (z). The mesh resolution near the cylinder and scour bed is 0.1 cm which is the finest resolution used by Smith and Foster (2005). Note that only one background mesh is needed for all bed profiles as the shape of the cylinder and scour bed profiles are embedded into the background mesh and automatically processed by the CFD model. A close-up view of the fluid and IB mesh cells is shown in Figure 3 after the cylinder and bed profile 3 geometry is embedded into the background mesh. The meshes for the two other profiles are similar.

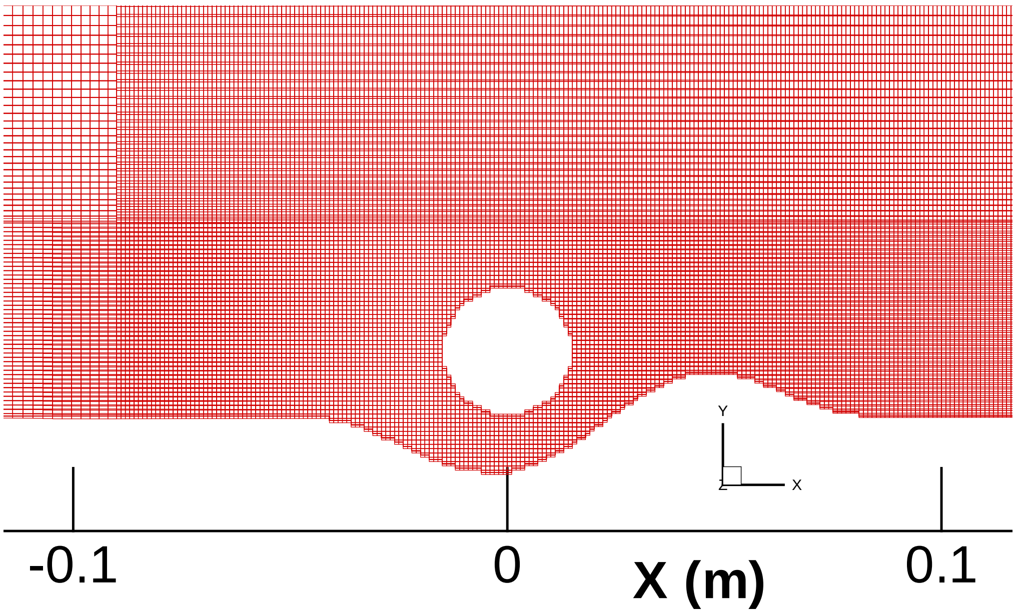

Figure 14. The fluid and IB mesh cells of the background mesh used in the terrain-embedding CFD modeling after the cylinder and scour bed geometry inserted.

Results and Discussion

Both terrain-conforming and terrain-embedding methods are used to simulate the case with the three bed profiles (1, 3 and 5). The CFD results are compared with each other and against the flume measured velocity data. These results are presented below to shed light on the two CFD methods.

The overall flow patterns for the three profiles are shown in Figure 4. The flow patterns are varying drastically with the changing bed profiles. A noteworthy feature is that the CFD results show that unsteady vortex shedding starts to develop with profile 5, while flows with profiles 1 and 3 remain steady. This result is consistent with the findings of Smith and Foster (2005).

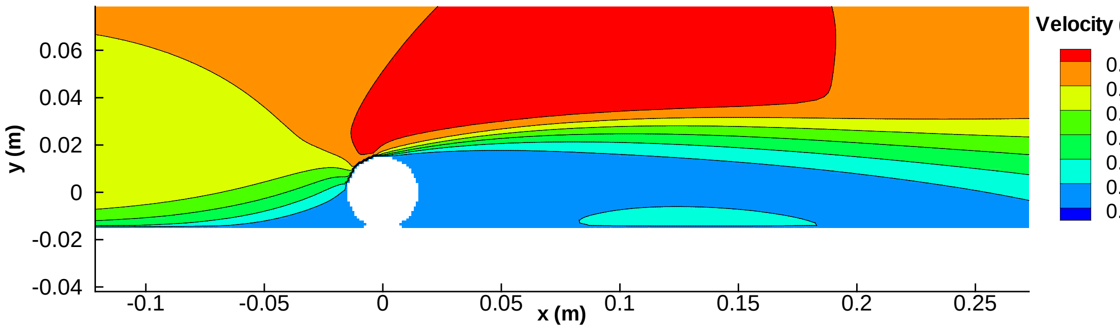

(a) Profile 1

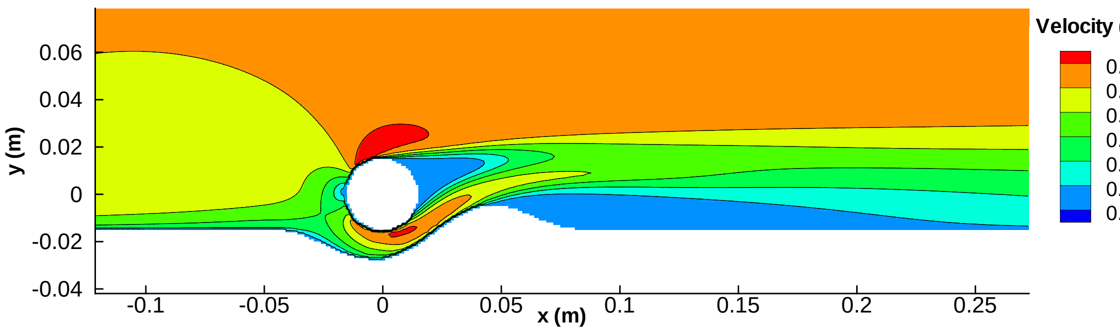

(b) Profile 3

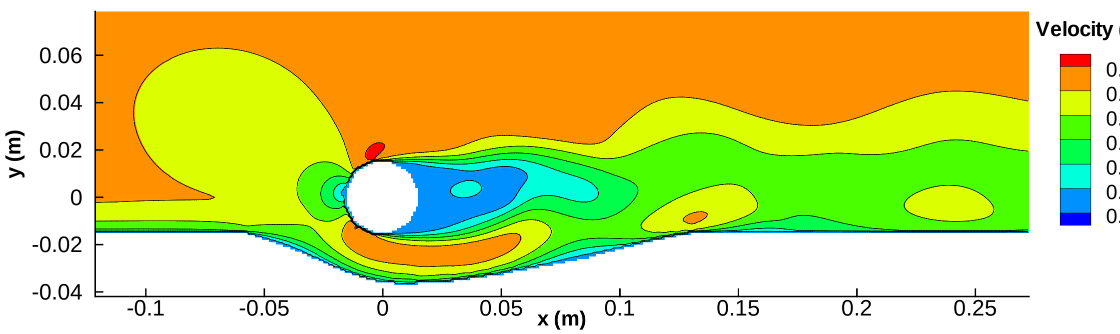

(c) Profile 5

Figure 15. CFD predicted velocity magnitude contours of the flow pattern with the terrain-embedding method.

The streamwise velocity component is compared in Figure 5 between CFD results and measured data. The flow approaches the cylinder with a near-logarithmic velocity profile with all cases and the CFD results agree with the measured data well. The impact of the cylinder is still significant even at the last measured station eight cylinder-diameters downstream (x=24 cm). The terrain-embedding CFD results agree with the measured data reasonably well for all three profiles and eight streamwise stations. The terrain-conforming CFD results agree also in most stations except for the three stations downstream of the cylinder for profile 3. The terrain-conforming method predicted a stronger flow near the bed downstream of the cylinder than the data, which significantly shortens the flow reversal in the zone. The mismatch is primarily caused by the inability of the model to resolve the ending of the jet and beginning of the flow separation on the upper and lower portions of the cylinder, leading to a different wake characteristic. It is unclear why the terrain-embedding CFD predicts the wake dynamics of profile 3 better than the terrain-conforming method. Probable causes may be due to the use of different wall functions as well as the different implementations of the wall-function. Wall-function will influence the predicted boundary layer as well as the separation locations. It is noted that the results obtained by Smith and Foster (2005) with FLOW-3D are similar to our results of the terrain-conforming modeling for profile 3.

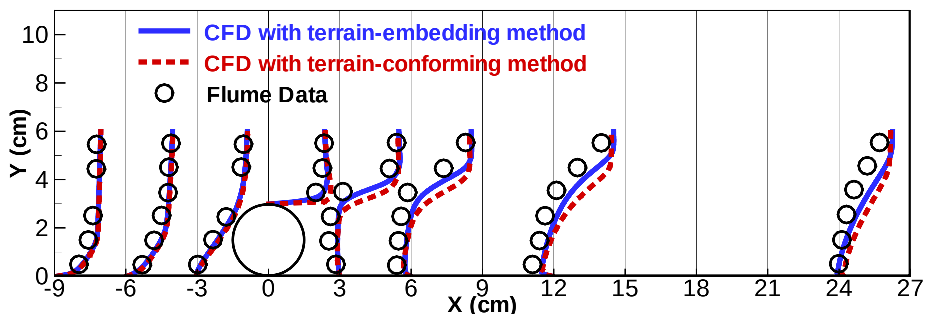

(a) Profile 1

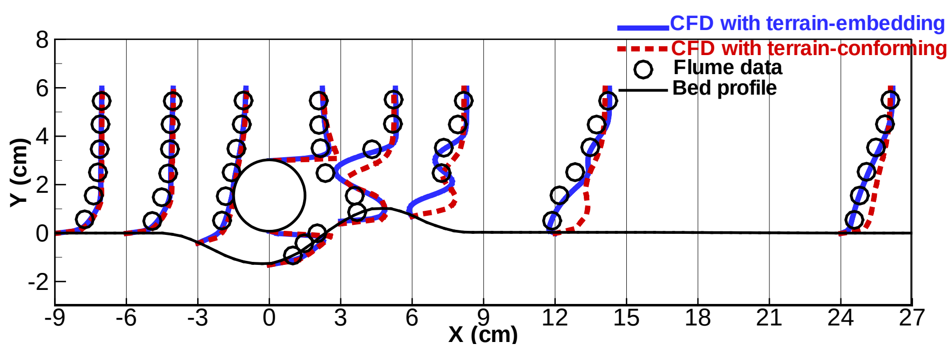

(b) Profile 3

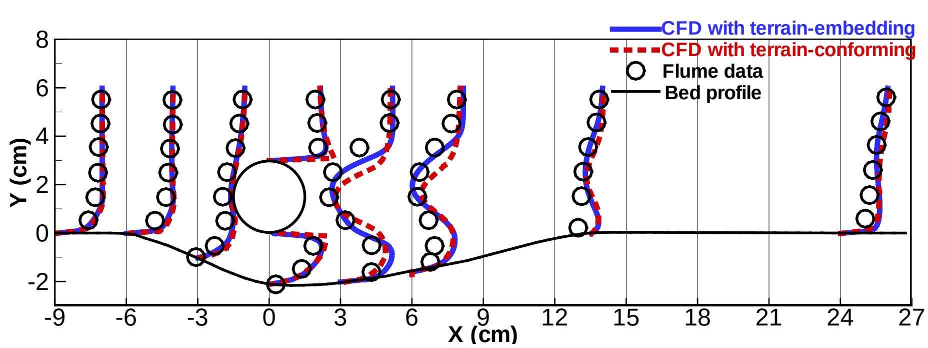

(c) Profile 5

Figure 16. Comparison of CFD and measured streamwise velocity components (U) along eight streamwise stations. Scaling of U is such as one unknit of X is 10 cm/s.

SUMMARY

A new terrain-embedding method is developed into the U^2RANS model of Lai et al. (2003). A flume case is simulated to compare both the terrain-embedding and terrain-conforming methods. It is found that the terrain-embedding method works well for the simulated case: (a) the mesh generation process is relatively simple; (b) the numerical simulation is stable; (c) the computing time is reduced as it was found that the convergence was faster than the terrain-conforming method; and (d) the simulated results are good in comparison with the measured data.

The study shows that the terrain-embedding method of U^2RANS has a great potential to be used for practical stream flow modeling with complex terrains. The greatest benefits of the method, compared with the traditional terrain-conforming method, are that the mesh generation is much simplified, and the good mesh quality may be maintained. These benefits point to the potential of the terrain-embedding method for predicting scour processes when the mesh of the scoured bed is moving. In such moving-mesh applications, the terrain-conforming method is known to be prone to numerical instability and degradation of model accuracy. The terrain-embedding method, however, will be expected to perform well, which will be our future research and development effort.

REFERENCES

ASCE (2007). ASCE Sedimentation Manual. Sedimentation Engineering: Processes, Measurements, Modeling and Practice. ASCE Manual and Reports on Engineering Practice No.110. Reston, VA. Marcelo Garcia (ed).

Behr, M., and Tezduyar, T. E. (1994). "Finite-element solution strategies for large-scale simulations." Comput. Methods Appl. Mech. Eng., 112, 3–24.

Berger, R. C., and Stockstill, R. L. (1999). "A finite-element system for flows." Proc., 1999 American Society of Civil Engineers (ASCE) Water Resources Engineering Conf., Water Resources into the New Millennium, Past Accomplishments and New Challenges, Seattle.

Bihs, H., Ong, M., Kamath, A. and Arntsen, Ø. A. (2013). "A level set method based numerical wave tank for calculation of wave forces on horizontal and vertical cylinders." In Proc., Seventh National Conference on Computation Mechanics, Trondheim, Norway.

Casulli, V. (1997). "Numerical simulation of three-dimensional free surface flow in isopycnal coordinates." Int. J. Numer. Methods Fluids, 25, 645–658.

Casulli, V. and Stelling, G.S. (1998). "Numerical simulation of 3D quasi-hydrostatic, free-surface flows." Journal of Hydraulic Engineering, 124(7):678–686.

Casulli, V. (1999). "A semi-implicit finite difference method for non-hydrostatic, free-surface flows." International Journal for Numerical Methods in Fluids, 30:425–440.

Demuren, A. O. (1993). "A numerical model for flow in meandering channels with natural bed topography." Water Resour. Res., 19(4),1269–1277.

Fringer, O.B., Gerritsen, M., and Street, R.L. (2006). "An unstructured-grid, finite-volume, nonhydrostatic, parallel coastal ocean simulator." Ocean Modeling, 14(3-4):139–173.

Ge, L., and Sotiropoulos, F. (2007). "A numerical method for solving the 3D unsteady incompressible navierstokes equations in curvilinear domains with complex immersed boundaries." J. Comput. Phys., 225(2), 1782–1809.

Jensen, B. L., Sumer, B. M., Jensen, H. R., and Fredsoe, J. (1990). Flow around and forces on a pipeline near a scoured bed in steady current. Journal of Offshore Mechanics and Arctic Engineering, 112(3), 206-213.

Jia, Y. (2013). Technical Manual of CCHE3D Version 1.1. NCCHE-TR-01-2013. National Center for Computational Hydroscience and Engineering, The University of Mississippi University, MS 38677.

Kang, S., Lightbody, A., Hill, C., and Sotiropoulos, F. (2011). "High resolution numerical simulation of turbulence in natural waterways." Adv. Water Resour., 34(1), 98–113.

Khosronejad, A, Kozarek, J.L., and Sotiropoulos, F. (2014). "Simulation-Based Approach for Stream Restoration Structure Design: Model Development and Validation." J. Hydraul. Eng., 140, (ASCE)0733-9429/04014042.

Lai, Y. G., Weber, L. J., and Patel, V. C. (2003). "Nonhydrostatic three dimensional method for hydraulic flow simulation. I: Formulation and verification.'' J. Hydraul. Eng., 129(3), 196–205.

Lai, Y.G. (2019). Three-Dimensional Stream Flow Modeling with a Smooth-Bed Z Mesh. World Environmental and Water Resources Congress, ASCE/EWRI, Pittsburg, PA, May 19-23, 2019.

Launder, B. E., and Spalding, D. B. (1974). "The numerical computation of turbulent flows." Comput. Methods Appl. Mech. Eng., 3, 269–289.

Liu, X. and Zhang, J. (editors) (2019). Computational Fluid Dynamics: Applications in Water, Wastewater, and Stormwater Treatment. ASCE Publications, 2019. https://doi.org/10.1061/9780784415313

Mahadevan, A., Oliger, J., and Street, R. (1996a). "A nonhydrostatic mesoscale ocean model. part i: Well-posedness and scaling." Journal of Physical Oceanography, 26(9):1868–1880.

Mahadevan, A., Oliger, J., and Street, R. (1996b). "A nonhydrostatic mesoscale ocean model. part ii: Numerical implementation." Journal of Physical Oceanography, 26(9):1881–1900.

Mao, Y. (1986). The interaction between a pipeline and an erodible bed. PhD thesis, Technical Univ. of Denmark, Lyngby, Denmark.

Olsen, N. and Melaaen, C. (1993). “Three-dimensional calculation of scour around cylinders.” J. Hydraul. Eng. 119(9): 1048–1054.

Olsen, N. (1994). “SSIIM: A three-dimensional numerical model for simulation of water and sediment flow.” HYDROSOFT 94, Porto Carras, Greece.

Olsen, N. and Kjellesvig, H.M. (1998). “Three dimensional numerical flow modeling for estimation of maximum local scour depth.” J Hydraul Res 36(4):579590.

Papanicolaou, A.N.T., Elhakeem, M., Krallis, G., Prakash, S., Edinger, J. (2008). “Sediment Transport Modeling Review - Current and Future Developments.” J. Hydraulic Engineering, ASCE, 134(1), 1-14.

Smith, H. D. and Foster, D. L. (2005). Modeling of flow around a cylinder over a scoured bed. Journal of waterway, port, coastal, and ocean engineering, 131(1), 14-24.

Song, Y., Lai, Y.G., and Liu, X. (2020). Improved adaptive immersed boundary method for smooth wall shear. ASCE World Environmental and Water Resources Congress, Henderson, NV, May 17-21, 2020.

Ullmann, S. (2008). “Three-dimensional computation of non-hydrostatic free-surface flows.” MS Thesis, Delft University of Technology.

Xu, Y. and Liu, X. (2019). An immersed boundary method with y+-adaptation wall function for smooth wall shear. Under review.